

REDMAPPER II: X-RAY AND SZ PERFORMANCE BENCHMARKS FOR THE SDSS CATALOG

E. ROZO¹, E. S. RYKOFF¹
Draft version October 9, 2018

ABSTRACT

We evaluate the performance of the SDSS DR8 redMaPPer photometric cluster catalog by comparing it to overlapping X-ray and SZ selected catalogs from the literature. We confirm the redMaPPer photometric redshifts are nearly unbiased ($\langle \Delta z \rangle \leq 0.005$), have low scatter ($\sigma_z \approx 0.006 - 0.02$, depending on redshift), and have a low catastrophic failure rate ($\approx 1\%$). Both the $T_X - \lambda$ and $M_{\text{gas}} - \lambda$ scaling relations are consistent with a mass scatter of $\sigma_{\ln M|\lambda} \approx 25\%$, albeit with a $\approx 1\%$ outlier rate due to projection effects. This failure rate is somewhat lower than that expected for the full cluster sample, but is consistent with the additional selection effects introduced by our reliance on X-ray and SZ selected reference cluster samples. Where the redMaPPer DR8 catalog is volume limited ($z \leq 0.35$), the catalog is 100% complete above $T_X \gtrsim 3.5$ keV, and $L_X \gtrsim 2 \times 10^{44} \text{ erg s}^{-1}$, decreasing to 90% completeness at $L_X \approx 10^{43} \text{ erg s}^{-1}$. All rich ($\lambda \gtrsim 100$), low redshift ($z \lesssim 0.25$) redMaPPer clusters are X-ray detected in the ROSAT All Sky Survey (RASS), and 86% of the clusters are correctly centered. Compared to other SDSS photometric cluster catalogs, redMaPPer has the highest completeness and purity, and the best photometric redshift performance, though some algorithms do achieve comparable performance to redMaPPer in subsets of the above categories and/or in limited redshift ranges. The redMaPPer richness is clearly the one that best correlates with X-ray temperature and gas mass. Most algorithms (including redMaPPer) have very similar centering performance, with only one exception which performs worse.

Subject headings: galaxies: clusters

1. INTRODUCTION

Galaxy clusters are well known cosmological probes (e.g. Henry et al. 2009; Vikhlinin et al. 2009b; Mantz et al. 2010a; Rozo et al. 2010; Clerc et al. 2012; Benson et al. 2013; Hasselfield et al. 2013). Indeed, galaxy clusters are a key component of the current efforts to probe our accelerating Universe with photometric surveys such as the Dark Energy Survey (DES, The DES Collaboration 2005), Pan-STARRS (Kaiser et al. 2002), the Hyper-Suprime Camera², and the Large Synoptic Survey Telescope (LSST, LSST Dark Energy Science Collaboration 2012). For these efforts to succeed, one requires a robust, well calibrated, fully optimized photometric cluster finding algorithm.

This work is a companion paper to Rykoff et al. (2013, henceforth Paper I), which introduces redMaPPer, a new optical cluster finding algorithm specifically designed to take full advantage of these upcoming photometric surveys. The primary goal of this work is to evaluate the performance of redMaPPer against a variety of X-ray and SZ selected catalogs. The motivation for this type of comparison is manifold.

First, while it is true that galaxy clusters were first discovered in the optical as far back as the 1800's (Biviano 2000), and that the first large cluster catalogs relied on optical observations (e.g. Abell 1958; Zwicky et al. 1968; Abell et al. 1989), ever since the 1990's photometric cluster selection has been viewed as relatively unreliable. In particular, optical selection is broadly con-

sidered to be prone to severe projection effects (Lucey 1983; Frenk et al. 1990; van Haarlem et al. 1997). While these early results were concerned with photometric cluster finding with single band imaging, the modern literature has clearly demonstrated that projection effects remain a critical concern for optically selected samples, even with the advent of multi-band data (e.g. Cohn et al. 2007; White et al. 2010; Noh & Cohn 2011; Angulo et al. 2012). While it has been argued that projection effects can be minimized through a careful treatment of photometric data (Roza et al. 2011, Paper I), it remains to be explicitly demonstrated that a low incidence of projection effects can be achieved. Because X-ray cluster selection is extremely robust to projection effects, a direct comparison of the redMaPPer catalog to X-ray selected systems and sources in the ROSAT All Sky Survey (Voges et al. 1999) allows us to directly test the incidence of severe projection effects in redMaPPer.

Second, it has long been recognized that photometric mass proxies such as total galaxy counts and/or total cluster luminosity may not be very effective. That is, while these quantities are clearly correlated with cluster mass, they appear to exhibit large scatter (Gladders et al. 2007; Roza et al. 2009a; Song et al. 2012). However, recent work has argued that optimized redshift estimators can deliver low scatter (Roza et al. 2009b; Rykoff et al. 2012), although the arguments have been based on noisy data with an intrinsically large scatter (though see also Andreon 2012). Here, we wish to explicitly test whether a scatter in mass at fixed richness as low as has been claimed in the literature can be realized by comparing the redMaPPer richness estimator against low-scatter X-ray mass proxies such as X-ray temperature and gas mass.

¹ SLAC National Accelerator Laboratory, Menlo Park, CA 94025.

² <http://www.naoj.org/Projects/HSC/HSCProject.html>

Third, it is sometimes suggested that optically selected clusters represent a fundamentally distinct population of galaxy clusters from X-ray and/or SZ selected galaxy clusters — the so-called X-ray underluminous systems — as opposed to X-ray and optically selected cluster samples having regular scaling relations (e.g., Donahue et al. 2001; Rasmussen et al. 2006; Lopes et al. 2009; Dai et al. 2010; Andreon & Moretti 2011; Balogh et al. 2011; Planck Collaboration 2011c; Wang et al. 2011; Roza et al. 2012c). Of course, in detail, no optical cluster catalog can be precisely the same as an X-ray or SZ selected catalog. Rather, the relevant question is whether the relative selection functions behave as expected. For instance, optically selected clusters cannot be detected in X-rays if they are fainter than the flux limit of the X-ray survey, so one naturally expects the fraction of optically selected clusters detected in X-rays to decline in a simple, predictable manner with both richness and redshift. Is this, in fact, the case? Similarly, are there any massive X-ray and/or SZ selected clusters which one would expect to be detected in optical, but which are not? Addressing these questions is of critical importance in cementing photometric cluster selection as a viable alternative to X-ray and SZ cluster surveys.

Of course, redMaPPer is far from the only cluster finding algorithm available in the literature today. At present, there exists a large variety of photometric cluster finding algorithms, with roughly half of the cluster finders relying on photometric galaxy redshifts for cluster identification (e.g., Kepner et al. 1999; van Breukelen & Clewley 2009; Milkeraitis et al. 2010; Durret et al. 2011b; Szabo et al. 2011; Soares-Santos et al. 2011; Wen et al. 2012) and half (including redMaPPer) relying on the red-sequence technique (Annis et al. 1999; Gladders & Yee 2000; Koester et al. 2007a; Gladders et al. 2007; Gal et al. 2009; Thanjavur et al. 2009; Hao et al. 2010). Given the variety of different algorithms and techniques employed in optical cluster finding, maximizing the utility of ongoing and near future photometric surveys necessitates a detailed comparison of these various algorithms. In this way, we may adequately identify which techniques are better or worse suited to the specific question at hand, in particular cluster cosmology. The secondary goal of this work then is to compare and contrast the performance of redMaPPer against that of several other cluster finders.

The basic analysis framework that we use for the comparison of redMaPPer to other cluster finding algorithms is fundamentally different than the type of cross-comparison work that has been performed in the past. Specifically, we do not directly compare redMaPPer against the other catalogs. The reason is simple: consider, for instance, comparing two photometric cluster catalogs A and B . If the richness comparison of catalogs A and B is noisy, how can one tell whether A is at fault, or whether B is at fault? If a specific cluster is found in catalog A , but not catalog B , does that constitute a failure of catalog A , a failure of catalog B , or neither, or both? Because one does not know *a priori* which catalog is “more correct” — and this needs to be properly defined — it is unclear what kind of inferences could be made from such a comparison (see e.g., Bahcall et al. 2003, for further discussion). What one needs to perform a proper comparison then is some sort

of “truth table”, i.e., a definition of “more correct”.

In this work, we rely on X-ray and SZ selected catalogs as a truth-table of sorts. So, for instance, given two optical catalogs A and B , we can unambiguously determine whether the fraction of galaxy clusters detected in X-rays is higher for catalog A than for catalog B or vice versa. Provided galaxy clusters form a single population with well defined scaling relations, then a larger fraction of X-ray selected clusters can be unambiguously viewed as a good thing. Similarly, a lower scatter in X-ray temperature and/or gas mass at fixed richness is also clearly a good thing, as both of these quantities are recognized as very accurate mass proxies.

In addition, it is our hope that as various features of photometric cluster finding algorithms are revealed to be more or less effective, that the field as a whole will converge into a more unified framework. As noted above, there are now at least 15 different cluster finding algorithms, all of which have different selection functions, and different richness and redshift estimators. Consequently, it is difficult to compare the results from various research groups, even more so given that each cluster finding algorithm is typically run on only one data set. By identifying which techniques are more or less effective, we hope the field can converge into a common language that will facilitate communication. Conversely, if we find that several techniques are all found equally effective, then there is a strong motivation to pursue multiple cluster detection avenues in future work, so as to provide an explicit test of cluster cosmology with several independent samples.

Our work is laid out as follows. In Section 2, we introduce the redMaPPer catalog, and the various X-ray and SZ catalogs that will be employed in our analysis of the performance of redMaPPer. Section 3 discusses how we match galaxy clusters across catalogs, a process that is the fundamental stepping stone for all subsequent work. Section 4 compares the redMaPPer redshifts to those of our reference catalogs, while Section 5 explore the X-ray and SZ scaling relations with the redMaPPer optical richness. Section 6 discusses the relative X-ray and SZ completeness and purity of the redMaPPer catalog, and section 7 evaluates the efficacy of the redMaPPer centering algorithm. Finally, in Section 8 we perform a simplified version of all of the above analyzes for all photometric cluster catalogs available in the SDSS (including redMaPPer). While this analysis is less thorough than that used for the detailed characterization of redMaPPer — in particular we do not perform extensive visual inspection of all cluster catalogs and their matches to the X-ray and SZ catalogs — the analysis is completely homogeneous: all cluster catalogs are treated in exactly the same way. Section 9 summarizes our results and present our conclusions. When necessary, distances are estimated assuming a flat Λ CDM model with $\Omega_m = 0.27$, and $h = 0.7$ Mpc.

2. CATALOGS

2.1. The SDSS DR8 redMaPPer Catalog

The **red**-sequence **M**atched-filter **P**robabilistic **P**ercolation (redMaPPer) algorithm (Paper I: Rykoff et al. 2013) is a photometric cluster finding algorithm based on the optimized richness estimator λ (Roza et al. 2009b; Rykoff et al. 2012). redMaPPer identifies galaxy

clusters as overdensities of red-sequence galaxies. It relies on an iterative self-training technique to fully characterize the evolution of the red sequence as a function of redshift, including zero-point, tilt, and scatter. As the algorithm utilizes all colors ($u - g$, $g - r$, $r - i$, and $i - z$) simultaneously, the “scatter” is characterized by a full covariance matrix. The algorithm then uses the resulting red sequence model, combined with simple radial and luminosity filters, to estimate the probability that any given galaxy belongs to any given cluster. The cluster richness λ is the sum of these probabilities. In addition, the algorithm estimates cluster photometric redshifts by simultaneously fitting all high probability cluster members with a single red sequence model.

The redMaPPer catalog used in this work is that obtained from running the algorithm on the SDSS DR8 data (Aihara et al. 2011). The survey mask is the same as that used for the Baryon Acoustic Oscillation Survey (BOSS) target selection (Dawson et al. 2013), supplemented by some additional cuts around unmasked bright stars and foreground galaxies (e.g. M31), for a total area of $\approx 10,000$ deg². All richness estimates are corrected for masked area due to survey edges, bright stars, and bad fields, and the catalog is further trimmed so that no cluster is masked by more than 20%. Spectroscopic redshifts used for photometric redshift training and validation are derived from a compilation of SDSS main (Strauss et al. 2002), luminous red galaxy (LRG, Eisenstein et al. 2001), and BOSS DR9 (Ahn et al. 2012) galaxy samples. For a detailed description of how the photometric and spectroscopic catalogs are used in the training and construction of the catalog, we refer the reader to Paper I.

2.2. X-ray and SZ Catalogs

The SDSS DR8 redMaPPer catalog will be compared to the X-ray and SZ catalogs described below. In all cases, we adopt a cut on data quality: if X is the cluster observable of interest (e.g. L_X , T_X , M_{gas}), we discard from the reference cluster catalog any systems with $\Delta X/X \geq 0.3$. The catalogs employed in our analysis are:

XCS: The XMM Cluster Survey (XCS: Mehtens et al. 2012) is a serendipitous search for galaxy clusters using all publicly available data in the *XMM-Newton* Science Archive. The first data release is comprised of 503 optically confirmed, serendipitously detected galaxy clusters. Of these, 261 have spectroscopic redshifts, and 203 have photometric redshift estimates. We restrict ourselves to the sub-sample of 402 galaxy clusters with temperature estimates. By necessity, the X-ray temperatures reported in the XCS catalog are not core-excised.

MCXC: The Meta-Catalog of X-ray detected Clusters of galaxies (MCXC: Piffaretti et al. 2011) is a compilation of galaxy clusters based on publicly available X-ray data from both the ROSAT All Sky Survey (RASS: Voges et al. 1999) and serendipitous searches in ROSAT pointed observations. The RASS contributing catalogs are NORAS (Böhringer et al. 2000), REFLEX (Böhringer et al. 2004), BCS (Ebeling et al. 1998), SGP (Crudace et al. 2002), NEP (Henry et al. 2006), MACS (Ebeling et al.

2001), and CIZA (Ebeling et al. 2002; Kocevski et al. 2007), while the contributing serendipitous catalogs are 160D (Mullis et al. 2003), 400D (Burenin et al. 2007), SHARC (Romer et al. 2000), WARPS (Horner et al. 2008), and EMSS (Gioia et al. 1990). The data from each of the individual galaxy catalogs was collected and homogenized, deleting duplicate entries, and enforcing a consistent X-ray luminosity definition. In the catalog, L_X is defined to be the X-ray luminosity in the 0.1–2.4 keV band within an R_{500c} aperture. Unfortunately, the catalog does not include errors in the X-ray luminosity estimates.

ACCEPT: The ACCEPT cluster catalog is a compilation of X-ray clusters with deep *Chandra* data (Cavagnolo et al. 2009). All data were independently reduced and homogeneously analyzed, with projected temperature radial profiles available for all galaxy clusters. However, a single core-excised X-ray temperature is not reported. We utilize the temperature and gas profiles to compute a spectroscopic-like core-excised temperature using the weighting scheme in Mazzotta et al. (2004). The necessary integrals from Mazzotta et al. (2004) are discretized into a sum over the observed radial bins, and core-excision is done using a 150 kpc aperture when possible. If no radial bins falls entirely outside this region, we do not perform core-excision.

Errors in the X-ray temperatures are estimated via direct Monte Carlo: the density and temperature profiles are randomly sampled based on their reported errors, and these are used to compute the average temperature as described above. The error is defined to be the standard deviation of the Monte Carlo samples for each cluster. Because ACCEPT reports their interpolated temperature profiles (so as to match their gas density profiles) there is significant covariance between neighboring radial bins. This leads to an under-estimate of the true temperature uncertainties in our Monte Carlo method. Unfortunately, the non-interpolated profiles were not available, so we simply assume that 1-off neighboring bins are perfectly correlated, with no covariance between non-neighboring bins. This increases our estimated error by a factor of $\sqrt{2}$, though we hasten to add that these errors have a negligible impact on the recovered scatter in X-ray temperature at fixed richness.

There is one cluster in this catalog that deserves special mention. Specifically, visual inspection of the density and temperature profiles of Abell 1942 reveals an obvious failure in the automated data reduction for $R \geq 500$ kpc, so including the information in the reported profiles beyond these radius severely biases the recovered X-ray temperature. Consequently, when estimating T_X for this system, we truncate all profiles at $R = 400$ kpc. We have explicitly verified with the ACCEPT team that truncating the integration at $R = 400$ kpc for this galaxy cluster is appropriate, and that failure to do so will introduce large systematic errors in the recovered X-ray temperature (M. Donahue 2012, private communication). We note that if we do not truncate the profiles at this radius for Abell 1942, then this cluster becomes a gross outlier in the T_X - λ relation (see section 5).

Mantz: The Mantz cluster sample (Mantz et al. 2010b) is comprised of galaxy clusters contained within the ROSAT Brightest Cluster Sample (BCS: Ebeling et al. 1998), the ROSAT-ESO Flux-Limited X-ray sample (REFLEX: Böhringer et al. 2004), and the bright sub-sample of the Massive Cluster Survey (Bright MACS: Ebeling et al. 2010). Clusters from each of these catalogs were selected by applying a redshift-dependent flux cut, so as to select the most luminous X-ray clusters in the various samples. A sub-sample of these galaxy clusters was observed with *Chandra* in order to derive X-ray temperatures and gas masses. Our analysis is restricted to this sub-sample of galaxy clusters with gas mass measurements.

Planck ESZ: The Planck all-sky Early Sunyaev-Zeldovich Cluster sample (Planck Collaboration 2011a) comprises 189 galaxy clusters detected with signal-to-noise $S/N \geq 6$ in the Planck early data release. Of these, 20 were newly detected clusters, most with perturbed morphologies in the X-rays. The clusters are typically massive low redshift clusters, with the effective mass threshold increasing with increasing redshift.

ROSAT Bright and Faint Source Catalogs: The ROSAT Bright (Voges et al. 1999) and Faint (Voges et al. 2000) Source Catalogs are comprised of all X-ray sources in the ROSAT All Sky Survey. X-ray detection is based on count rate in the 0.1–2.4 keV band, but sources must also pass likelihood thresholds, and have a minimum number of photon counts. The resulting catalog has over 10^5 X-ray sources over the entire sky.

2.3. Richness and Photometric Redshift Estimates of Clusters in the Reference Catalogs

To facilitate cross-catalog matching, we explicitly measure the richness and photometric redshift of every cluster in our reference catalogs that falls within our DR8 galaxy mask. In doing so, we hold the center of the galaxy clusters fixed to the reported X-ray centers. We estimate the cluster richness λ in exactly the same way as we do for clusters detected in the redMaPPer catalog, as described in Paper I. We note that while we hold the cluster center fixed, when estimating cluster richness we do not rely on the reported cluster redshifts in the reference catalogs, but rather estimate the photometric redshift z_λ from the photometric data. When measuring richness, the reported cluster redshift is only employed when initializing our iterative photometric redshift estimate algorithm.

3. CLUSTER MATCHING

Throughout this work, we will be comparing the properties of the X-ray/SZ-selected cluster catalogs to the redMaPPer clusters, so we must first define an algorithm for matching galaxy clusters between different cluster catalogs. We consider two types of matching algorithms, namely cylindrical (or proximity) matching, and membership matching.

3.1. Cylindrical Matching

Cylindrical matching is simple: given a cluster $x \in X$, we wish to find the corresponding cluster match $y \in$

Y . We rank order all clusters $x \in X$, and then find all clusters y within some physical radius R_{\max} (evaluated at the redshift z_x of cluster x) and within some maximum redshift offset Δz_{\max} . Here, we set $R_{\max} = 1.5$ Mpc and $\Delta z_{\max} = 0.1$, and the redshift is always that reported in the original catalogs (as opposed to our own photometric redshift estimate). If more than 2 clusters $y \in Y$ fall within the cylinder centered on x , we take the largest of the 2 as the correct match, and remove this cluster from consideration when matching subsequent clusters in X . Thus, all cluster matches are unique.

The above procedure defines the cluster match y of a cluster x . Using a similar algorithm, we can then find the cluster match \tilde{x} of the cluster y , which may or may not be the same as the original cluster x . Matches are considered spurious if $\tilde{x} \neq x$, and are dropped from the matched cluster list.

3.2. Membership Matching

Membership matching follows the same general algorithm to enforce unique, two-way matches between the X and Y cluster catalogs — i.e. we first match Y to X and then X to Y , keeping only clusters which are two-way matches. The main difference is the criterion used to match a cluster y to a cluster x . Specifically, let p_i^x be the probability that galaxy i belongs to cluster $x \in X$, and p_i^y be the probability that galaxy i belongs to cluster $y \in Y$. We define the matching strength $s(x,y)$ between two clusters x and y via

$$s(x,y) = \sum_i p_i^x p_i^y. \quad (1)$$

The match y to cluster x is that which maximizes the function $s(x,y)$ at fixed x . Likewise, the cluster match \tilde{x} to cluster y is that which maximizes $s(x,y)$ at fixed y . As before, if $\tilde{x} \neq x$ then the match is considered spurious and dropped from the list of matching clusters.

3.3. Testing The Matching Algorithms

For the vast majority of our clusters, the results from the cylindrical and membership matching agree. For each of our reference catalogs, we visually inspect all clusters for which the cylindrical and membership matches disagree. When possible, any such ambiguous cluster matchings are resolved based on our visual inspection. These disagreements are relatively rare, occurring in $\lesssim 5\%$ of all clusters. Notes for each of these systems are collected in Appendix A.

Additionally, recall that we have estimated the cluster richness for every cluster in our reference cluster catalogs. One should expect that all such clusters that satisfy the redMaPPer richness cuts should be matched to an existing cluster in the redMaPPer catalog. We find that there are a total of 9 galaxy clusters across all catalogs which were unmatched. None of these are unmatched due to a failure of the matching algorithms.

Specifically, one cluster is unmatched because it falls within an unmasked region in the SDSS with bad photometry. Three of the remaining eight are unmatched because they formally fall outside the redMaPPer angular selection threshold — i.e. their location on the sky is such that more than 20% of the cluster is masked out. The remaining five galaxy clusters have richnesses

that are very close to the richness threshold applied, and therefore scatter in and out of the sample due to the small differences in redshift and/or cluster centers between the redMaPPer and reference catalogs.

It is worth noting that these results also allow us to estimate the optical completeness, i.e. the fraction of galaxy clusters that pass our selection threshold but are not in the catalog due to catastrophic failures in the optical data and/or algorithm. Since there are 372 clusters MCXC satisfying our cuts, only one of which is rightfully unmatched due to bad photometry, we conclude that our optical incompleteness is $\lesssim 0.3\%$. Notes on each of the nine clusters noted above are collected in Appendix B.

4. REDSHIFT COMPARISONS

We begin by comparing the redMaPPer photometric redshift (“photo- z ”) estimator (z_λ) to the redshifts quoted in the reference catalogs. This is a necessary first step; all cluster observables derived using an incorrect redshift will be systematically biased, and will therefore compromise the study of cluster scaling relations, completeness, purity, etc. Consequently, when comparing redMaPPer to other catalogs, our first task must be to identify catastrophic redshift outliers.

For each matched cluster in our reference catalogs, we calculate the redshift offset $\Delta z = z_\lambda - z_{\text{ref}}$ of each cluster. For the photometric redshift z_λ , we consider both the photometric redshift estimate obtained while holding the cluster center of the reference cluster fixed (see section 2.3), and the cluster redshift of the redMaPPer cluster match.

The clusters are binned in redshift (based on our photometric redshift), and we require the bins be sufficiently wide to contain at least 25 clusters per bin. We focus on the redshift span $z \in [0.1, 0.5]$ over which the redMaPPer richness estimates are most robust. At $z \geq 0.5$, richness errors become very large due to the extrapolation in luminosity between the SDSS depth and the luminosity cut of $0.2L_*$ used to define λ .

As shown in Figure 1, the resulting distribution of redshift offsets typically exhibits a Gaussian core with possibly a few outliers. The parameters for the Gaussian core are estimated using the median redshift offset for the mean, and $1.4826 \times MAD$ for the standard deviation, where MAD is the median absolute deviation of the sample about the median.³ All 4σ outliers are identified and discussed. An example of the distribution of redshift offsets for the MCXC catalog, along with the recovered Gaussian fit and 4σ cuts is shown in Figure 1.

Our results are summarized in Table 1. The photo- z performance is consistent with that quoted in Paper I, that is, our redshifts are unbiased at the $\lesssim 0.005$ level, with scatter that is ≈ 0.008 for $z \lesssim 0.3$, but increasing to ≈ 0.02 by $z \approx 0.5$. The redMaPPer photometric failure rate is small, with two redshift failures for the full MCXC cluster catalog, and two clusters with bad photometry. The corresponding total failure rate (including bad photometry) is $\approx 1.2\% \pm 0.6\%$. The photo- z performance is largely insensitive to the choice of cluster center, though differences can arise if cluster centers are separated by large ($R \sim 1$ Mpc) offsets. Comments for

each of the galaxy clusters identified as outliers can be found in Appendix C.

5. X-RAY AND SZ SCALING RELATIONS

5.1. Methods

We now consider the efficacy of the redMaPPer richness λ as a mass tracer by looking at cluster scaling relations. To decouple this analysis from the performance of our optical centering algorithm, we rely on the cluster richness measurements at the reported cluster center in the reference catalogs. Cluster centering will be addressed in Section 7. Because both richness and X-ray observables depend on redshift, we remove all redshift outliers from this analysis. These are dominated by erroneous redshifts in the reference catalogs, but include four redMaPPer clusters. Note that the richness measurements are evaluated at our estimated photometric redshift, and not the reported cluster redshifts of the reference catalogs, so noise associated with photometric redshift uncertainties are included in our analysis. Finally, we impose two data cuts: the first is that the cluster richness must pass the redMaPPer selection criteria, and the second is that the error in the external observable (L_X , T_X , etc) must be less than 30%. The latter cut impacts primarily XCS galaxy clusters with relatively few photon counts.

The mean and scatter of the X-ray scaling relations are estimated using a standard Bayesian fitter (e.g., Rozo et al. 2012a; Kelly 2007) with a uniform prior on the amplitude, slope, and variance of the relation. These fits are performed in redshift bins, which are chosen to match those in Section 4. Errors are estimated via bootstrap resampling.

To check for possible systematic failures of redMaPPer, and/or identify unique galaxy clusters, we have also implemented an automated outlier rejection criteria. We reject from our fit all 3σ outliers in the scaling relation. There are only two such outliers, which are discussed below. For now, we simply note that we believe that exclusion of these clusters from our fits is well justified.

Of particular interest to us are estimates of the scatter in mass at fixed richness, which can be inferred from the scatter in X-ray/SZ observables at fixed richness as laid out in the Appendix of Rozo et al. (2012b). For simplicity, we assume zero intrinsic covariance between the various X-ray and SZ observables and the cluster richness. Setting the correlation coefficient r between λ and the additional observable X to $r = 0$ in Eq. A13 of Rozo et al. (2012b), we find that the scatter in mass at fixed richness is given by

$$\sigma_{M|\lambda}^2 = \frac{\sigma_{X|\lambda}^2}{\alpha_{X|M}^2} - \sigma_{M|X}^2 \quad (2)$$

where $\alpha_{X|M}$ is the slope of the observable–mass relation for the reference catalog. If $r \neq 0$, the scatter can be larger or smaller depending on the sign of r . For estimating the mass scatter, we adopt a fiducial scatter in mass at fixed $M_{gas}/T_X/L_X$ of 10%/15%/25% and slopes of $\alpha = 1.1, 1.5$, and 1.6. These numbers are characteristic of the vast literature on cluster scaling relations (e.g. Vikhlinin et al. 2009a; Mantz et al. 2010b; Pratt et al. 2009; Mahdavi et al. 2012; Rozo et al. 2012c, and many

³ The factor 1.4826 relates the MAD to the standard deviation for a Gaussian distribution.

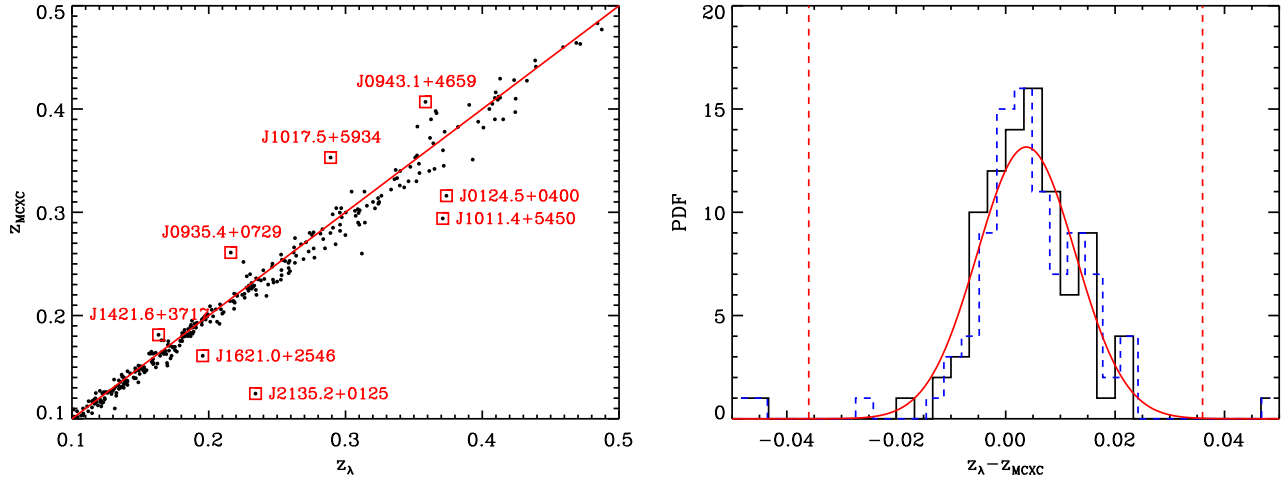


Figure 1. *Left panel:* Comparison between the MCXC redshifts and the redshifts of the matching redMaPPer clusters. Labeled clusters are flagged as outliers, and are dominated by erroneous redshifts in the MCXC catalog (see Appendix C). *Right panel:* Distribution of $\Delta z = z_\lambda - z_{\text{MCXC}}$ in the redshift bin $z_\lambda \in [0.2, 0.3]$. z_λ is either the photometric redshift at the reported center (black histogram) or the redshift of the matching redMaPPer cluster (blue dashed histogram). The apparent left–right offset of the two histograms arises because we have utilized two slightly different binning schemes to help differentiate between the two histograms. The red curve is the best fit Gaussian to the black histogram, and the dashed red-lines mark the 4σ cut employed to identify outliers.

Table 1
Comparison of redMaPPer Photo- z s to Reference Catalogs

Catalog	Redshift Bin	$\langle z_\lambda - z_{\text{ref}} \rangle$	σ_z	Tot. Cl.	Bad z_{ref}	Bad z_λ
XCS: fixed center	[0.1,0.3]	0.0038	0.0089	41	1	—
	[0.3,0.5]	0.0064	0.0192	44	—	—
XCS: matched	[0.1,0.3]	0.0043	0.0120	41	1	—
	[0.3,0.5]	0.0067	0.0206	44	—	—
MCXC: fixed center	[0.1,0.2]	0.0021	0.0057	163	1	—
	[0.2,0.3]	0.0037	0.0089	91	3	—
	[0.3,0.5]	0.0053	0.0170	75	2	—
MCXC: matched	[0.1,0.2]	0.0023	0.0050	163	2	—
	[0.2,0.3]	0.0041	0.0083	91	3	—
	[0.3,0.5]	0.0053	0.0170	75	2	2
ACCEPT: fixed center	[0.1,0.5]	0.0055	0.0094	56	2	—
ACCEPT: matched	[0.1,0.5]	0.0050	0.0080	56	2	—
Mantz: fixed center	[0.1,0.3]	0.0043	0.0067	31	—	1
Mantz: matched	[0.1,0.3]	0.0031	0.0057	31	—	1
Planck ESZ: fixed center	[0.1,0.5]	0.0030	0.0092	38	1	—
Planck ESZ: matched	[0.1,0.5]	0.0025	0.0081	38	1	—

Note. — “Fixed center” means the photometric redshift was estimated while holding the cluster center fixed to that reported in the reference catalog. “Matched” means we compare the redshift in the reference catalog to that of the matching redMaPPer cluster. σ_z is the width of the Gaussian core of the $P(\Delta z)$ distribution. “Tot. Cl.” is the total number of clusters in the redshift bin. “Bad z_{ref} ” is the number of 4σ outliers due to erroneous redshifts in the reference catalog. “Bad z_λ ” is the number of erroneous redMaPPer redshifts. The statistics in this table do not include two redMaPPer clusters that were compromised due to bad SDSS photometry.

others).

We emphasize that *the scaling relations presented in this work have not been corrected for selection effects.* This is because of two important considerations: first, our immediate goal is to quickly evaluate the performance of redMaPPer, leaving precise estimates of cluster scaling relations for future works (e.g. Greer et al, in preparation). Most importantly, though, the selection functions of our reference catalogs are often either

difficult to quantify without the tools employed in the construction of these catalogs (e.g. XCS, Planck ESZ), or downright impossible to quantify because the catalogs are aggregates from multiple sources (e.g. MCXC and ACCEPT). For the remaining Mantz catalog, our reliance on M_{gas} rather than L_X as the mass tracer implies that a proper treatment needs to account for the obvious covariance between these two X-ray observables, an analysis which is beyond the scope of this work.

In this context, it is important to note that systematic offsets in our recovered scaling relations scale with the variance of the relation. Thus, as long as this scatter is small, our recovered relations should be relatively robust to selection effects. As we will see below, both the T_X - λ and M_{gas} - λ scaling relations have small scatter ($\approx 20\% - 23\%$), so we expect these relations to be relatively unbiased. The same cannot be said of the L_X - λ relation, which exhibits a very large scatter ($\approx 70\%$).

5.2. Results

Our results are summarized in Table 2. We again caution that we expect the L_X - λ relation to be subject to large corrections from selection effects. A proper treatment can be found in Rykoff et al. (2012). We do not recommend drawing any conclusions from the L_X - M relation quoted here; we have included this information for completeness purposes only, and we will not discuss it further.

The left panel in Figure 2 shows the T_X - λ relation as probed by the XCS and ACCEPT cluster catalogs. The slopes and scatters of the two relations are consistent with each other, but their amplitudes are not. The amplitude offset at the geometric mean of the pivot point of the two samples is 0.35. That is, the two data sets exhibit a $\approx 40\%$ systematic offset in X-ray temperatures. This is unusually large, but there are many differences between the two X-ray temperature definitions, including the fact that the ACCEPT temperatures are core-excised whereas the XCS temperatures are not. Consequently, we are not particularly concerned with the XCS-ACCEPT offset. Rather, the most significant result from this comparison is that the scatter in mass at fixed richness inferred from the two samples are consistent with each other. We compute the inverse variance weighted mean of the inferred mass scatter from the XCS and ACCEPT catalogs to arrive at $\sigma_{\ln M|\lambda} = 0.26 \pm 0.03$.

We can compare these results to those derived from the M_{gas} - λ relation as probed by the Mantz galaxy clusters, shown in the right panel of Figure 2. The inferred mass scatter from this sample is $\sigma_{\ln M|\lambda} = 0.21 \pm 0.04$, also consistent with the XCS and ACCEPT values. The inverse variance weighted mean from the M_{gas} and T_X analysis is $\sigma_{\ln M|\lambda} = 0.24 \pm 0.02$. We expect selection effects can impact the scatter by $\approx \pm 0.05$, so $\sigma_{\ln M|\lambda} = 0.24 \pm 0.05$ is a more reasonable estimate of the scatter in mass at fixed richness.

These results are in excellent agreement with those of Rykoff et al. (2012). Relative to that work, our analysis benefits from our reliance on low-scatter mass proxies, albeit at the expense of introducing systematic uncertainties due to selection effects. In this context, we note that while the inferred mass scatter from the L_X - λ relation in this work appears to be larger than that inferred from the T_X - λ and M_{gas} - λ relations, we do not consider this problematic; The proper analysis of the L_X - λ relation in Rykoff et al. (2012) is consistent with a $\approx 25\%$ scatter in mass at fixed richness. We note that our estimate for the scatter is comparable to that achieved by current SZ experiments (Benson et al. 2013; Hasselfield et al. 2013).

5.3. Richness Failures

There are a total of two outliers over the full XCS, MCXC, ACCEPT, and MANTZ cluster samples.

XCS J1203.8+0147: This cluster is the neighbor of a much brighter X-ray foreground cluster. A reanalysis of the cluster by the XCS collaboration has resulted in significantly larger uncertainties in the recovered temperature, with $\Delta T_X/T_X = 0.46$. This new error estimates disqualifies the cluster from our sample, and strongly suggests that deeper X-ray data and a detailed multi-source analysis that deblends the foreground cluster is required if this system is to be included in our analysis.

400d J1416.4+4446: This cluster was initially reported in Vikhlinin et al. (1998), along with a spectroscopic redshift of $z = 0.400$. Visual inspection of the cluster reveals south-easterly and south-westerly extensions of the cluster galaxies, both of which are also apparent in a recent weak lensing analysis (Israel et al. 2012). Based on SDSS spectra, the redshift of these components are $z = 0.390$ and $z = 0.373$, suggesting these are cluster super-positions contained within a larger super-cluster. There is also an additional more distant southerly structure at $z = 0.397$. In short, this is a clear projection effect in the optical.

It is difficult to estimate the failure rate in our richness measurements from this data. The outlier fractions for XCS, ACCEPT, and Mantz galaxy clusters are 1/49, 0/54, and 1/29 respectively, though only one of these failures is due to a redMaPPer failure. This suggests a $\approx 1\%$ failure rate due to projection effects in the redMaPPer catalog. This failure rate is in addition to the $\approx 0.7\%$ photometric redshift failure rate.

5.4. SZ Comparison

We now turn to a comparison of redMaPPer clusters to the Planck ESZ cluster catalog. In this comparison, we have opted not to attempt to constrain the Y_{SZ} - λ scaling relation directly. This is for two primary reasons. First, because of its broad beam, the Planck centering errors are typically very large, which can strongly bias the richness measurements at the Planck centers. Second, the Y_{SZ} values derived solely from the Planck early data are both biased and very noisy (Planck Collaboration 2011b). Therefore, we leave a detailed analysis based on SZ follow-up of individual galaxy clusters to a future work (Greer et al, in preparation).

In light of these difficulties, we have opted instead to check the completeness of the Planck ESZ cluster sample. Figure 3 shows the Planck signal-to-noise as a function of cluster richness for all clusters in the DR8 footprint, evaluated at the Planck center. Although the vast majority of the clusters are very rich ($\lambda \gtrsim 70$), there are two clusters that stand out as unusually poor: PLCKG228.5+53.1 (ZwCl 1023.3+1257) and PLCKG182.6+55.8 (Abell 963). Both clusters have obvious central galaxies and both are strongly miscentered by Planck, with the radial offsets being 1.0 Mpc (6.4 arcmin) and 0.6 Mpc (3.0 arcmin) respectively. Both clusters are properly centered in the redMaPPer catalog, but even then their richnesses are relatively modest, $\lambda = 35.5$ and $\lambda = 30.5$ respectively.

Given their low richness, the detection by Planck of these two galaxy clusters is somewhat surprising. Visual inspection of the SDSS image of PLCKG228.5+53.1

Table 2
X-ray Scaling Relations with Richness

Catalog	Redshift Bin	λ_{pivot}	Amplitude	Slope	Scatter	Eq. Mass Scatter	Outlier Fraction
XCS	[0.1,0.3]	40.9	1.129 ± 0.056	0.56 ± 0.14	0.194 ± 0.055	0.25 ± 0.09	1/25
XCS	[0.3,0.5]	49.7	1.283 ± 0.071	0.57 ± 0.15	0.234 ± 0.062	0.32 ± 0.10	0/24
XCS	[0.1,0.5]	45.6	1.206 ± 0.044	0.57 ± 0.10	0.225 ± 0.042	0.30 ± 0.07	1/49
MCXC	[0.1,0.2]	48.9	0.289 ± 0.053	1.23 ± 0.12	0.66 ± 0.04	0.32 ± 0.03	0/159
MCXC	[0.2,0.3]	65.5	0.927 ± 0.086	1.24 ± 0.13	0.77 ± 0.07	0.41 ± 0.05	0/85
MCXC	[0.3,0.5]	62.9	0.818 ± 0.082	1.57 ± 0.11	0.64 ± 0.06	0.32 ± 0.04	0/71
MCXC	[0.3,0.5]	52.3	0.478 ± 0.041	1.38 ± 0.07	0.70 ± 0.03	0.36 ± 0.02	0/326
ACCEPT	[0.1,0.5]	94.5	1.905 ± 0.032	0.407 ± 0.066	0.196 ± 0.021	0.253 ± 0.036	0/54
Mantz	[0.1,0.5]	106.0	0.062 ± 0.052	0.72 ± 0.12	0.212 ± 0.032	0.210 ± 0.040	1/29

Note. — Amplitude, slope, and scatter refer to the X - λ scaling relation, where X is the relevant X-ray observable, i.e. T_X for XCS and ACCEPT, M_{gas} for Mantz, and L_X for MCXC. Our convention is $\langle \ln X | \lambda \rangle = A + \alpha \ln(\lambda/\lambda_{\text{pivot}})$ where A is the amplitude, α is the slope, and λ_{pivot} is taken to be the median cluster richness. “Eq. Mass Scatter” refers to the scatter in mass at fixed richness estimated based on the observed X-ray scaling relation as described in the text. We emphasize the L_X - λ relation suffers from large systematic errors due to unmodeled selection effects.

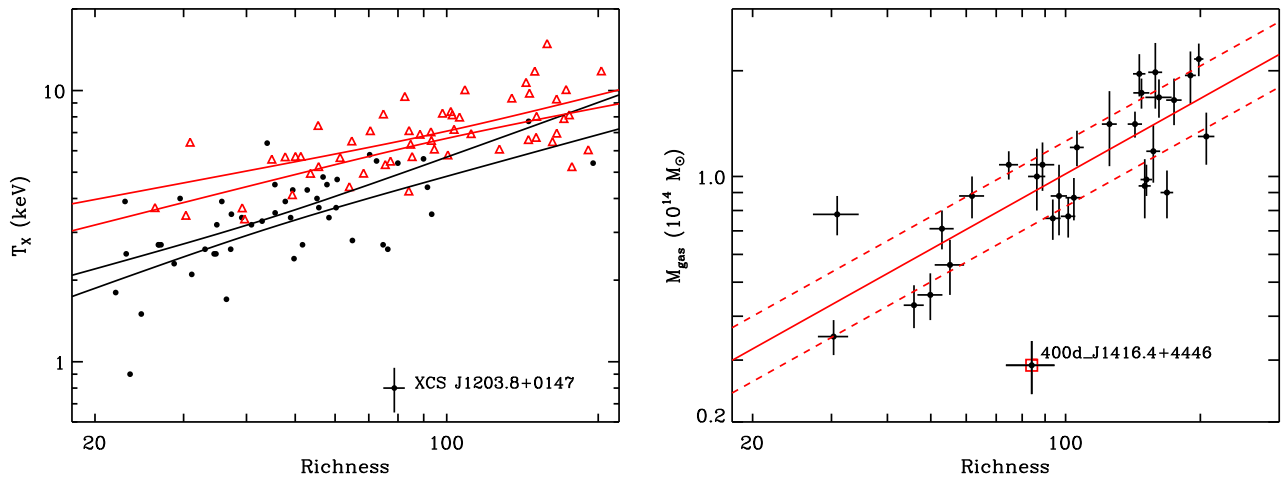


Figure 2. *Left panel:* The T_X - λ relation for XCS (black points) and ACCEPT (red triangles) galaxy clusters. Errors not shown to avoid cluttering the plot. The bands show the uncertainty in the mean relation. We note the two data sets exhibit a $\approx 40\%$ systematic offset in X-ray temperatures. This is due to several reasons, including the fact that the ACCEPT temperatures are core-excised while the XCS temperatures are not. *Right panel:* The M_{gas} - λ relation for Mantz galaxy clusters. The solid line shows the mean relation, and the dashed lines show the intrinsic scatter. The labeled galaxy clusters are gross outliers, and are discussed in the text. The inferred mass scatter from this sample is $\sigma_{\ln M|\lambda} = 0.21 \pm 0.04$.

reveals a possible very high redshift galaxy cluster just North of the quoted Planck center ($z_{\text{photo}} = 0.68 \pm 0.04$), which suggests that this detection may in fact be a high redshift system which was mistakenly associated with the low redshift cluster about 1.0 Mpc away. Deep optical follow-up of this field is desirable to either confirm or rule out this hypothesis.

The second of the two clusters, Abell 963, is also part of the ACCEPT and Mantz cluster catalogs. This is a cool-core relaxed galaxy cluster, and is also a known strong-lensing system. Looking at the T_X - λ relation from ACCEPT, and at the M_{gas} - λ relation from the Mantz catalog, we find that Abell 963 is both the hottest *and* largest M_{gas} cluster relative to its richness in each of these two cluster samples. Given that the SZ signal is proportional to $T_X \times M_{\text{gas}}$, it is not surprising that Abell 963 was

detected by Planck despite its relatively low optical richness. We have not explored whether this type of strong covariance between M_{gas} and T_X is generic, or whether the high thermal pressure in Abell 963 is fortuitous. Note that even though Abell 963 is the hottest and most gas-rich cluster relative to its richness, it is not an outlier, being only 2σ away from the expected T_X and M_{gas} values.

6. COMPLETENESS AND PURITY:

6.1. X-ray and SZ Completeness

The completeness of a cluster catalog may mean many different things depending on the context. As noted in Section 3, all except one of the reference galaxy clusters which satisfy the redMaPPer selection threshold are detected by redMaPPer, implying that the optical incom-

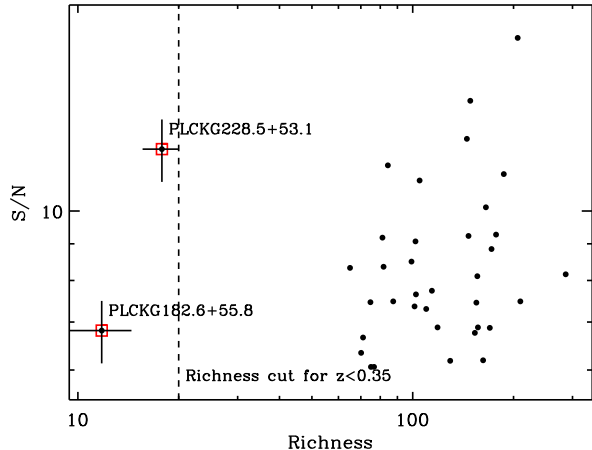


Figure 3. Signal-to-noise vs. richness for the Planck Collaboration (2011a) cluster sample. Richness is evaluated at the center reported in Planck Collaboration (2011a), which can be significantly offset from the true cluster center. The two highlighted clusters are unusually poor and are discussed in the text.

pleteness — i.e., the fraction of objects that we should have detected but failed to so — is $\lesssim 0.3\%$.

In this section, we ask a different question: given all XCS and ACCEPT galaxy clusters with $T_X \geq T_{\min}$, what fraction of these systems are included in the SDSS DR8 redMaPPer cluster catalog? In addressing this question, we remove from consideration all redshift outliers, both because this failure rate has already been characterized, and because redshift errors in the reference or redMaPPer catalogs will compromise the relevant mass tracers (λ , T_X , etc.).

The left panel in Figure 4 shows the fraction of XCS and ACCEPT galaxy clusters found in the redMaPPer catalog, as a function of the temperature threshold T_{\min} . As before, we limit ourselves to well measured clusters, with $\Delta T_X/T_X \geq 0.3$. At low redshifts, where the redMaPPer catalog is volume limited, we detect all X-ray clusters with $T_X \gtrsim 3.5$ keV. For $z \geq 0.35$ the increasing detection threshold for redMaPPer systems necessarily increases the minimum temperature over which we achieve 100% completeness. Over the redshift bin $z \in [0.3, 0.5]$, this minimum temperature is $T_X \gtrsim 5$ keV.

The right panel in Figure 4 shows the fraction of MCXC galaxy clusters detected by redMaPPer as a function of the luminosity threshold L_X . While the $z \in [0.1, 0.2]$ and $z \in [0.3, 0.5]$ bins suggest that redMaPPer is 100% complete above $L_X \gtrsim 2 \times 10^{44}$ erg s $^{-1}$, we find two clusters in the $z \in [0.2, 0.3]$ bin above this luminosity which were not matched. We visually inspected both of these systems:

MCXC J1326.2+1230: There is a very small ($\lambda \approx 11$) group at the reported location. The cluster is also identified in MCXC as Abell 1735. However, the reported position is very distant from Abell 1735, which is easily detected by redMaPPer ($\lambda = 81.4$). We assume the reported luminosity is appropriate for Abell 1735, in which case this cluster is in fact properly identified in redMaPPer.

MCXC J0927.1+5327: This cluster is clearly miscentered in the optical, which has caused the richness to fall below the detection threshold. Thus, this cluster is less a failure to detect than it is a case of cluster miscentering. In Figure 4, the drop in completeness at $L_X \approx 3.5 \times 10^{44}$ erg/s is due to this cluster.

In light of these findings, we have matched cluster MCXC J1326.2+1230 to redMaPPer assuming the cluster should be at the location of Abell 1735. The $z \in [0.2, 0.3]$ curve plotted in Figure 4 includes this correction, and demonstrates that redMaPPer is 100% complete for $L_X \gtrsim 2 - 4 \times 10^{44}$ erg s $^{-1}$ clusters.

We have performed a similar analysis using the galaxy clusters in the Mantz and Planck ESZ catalogs. We find that redMaPPer is 100% complete with respects to both of these catalogs. One galaxy cluster deserves special mention though: cluster PLCKG96.9+52.5 is clearly a rich ($\lambda = 76.7$) galaxy cluster that is not included in our SDSS redMaPPer cluster catalog. Nevertheless, we do not consider this galaxy cluster a redMaPPer failure. When centered at the Planck reported center, the SDSS galaxy mask is such that 17% of the galaxy cluster area is masked. However, this Planck cluster has a significant offset relative to the correct cluster center, which is obvious upon visual inspection, and is correctly identified by the redMaPPer algorithm. At that location, the mask fraction for the cluster is $\geq 20\%$, thereby failing to pass the redMaPPer cut. In other words, at the correct cluster center, cluster PLCKG96.9+52.5 does not fall within the angular mask used to define the redMaPPer catalog.

6.2. Purity

We now consider the converse of the question we addressed section 6.1: what fraction of redMaPPer galaxy clusters are X-ray detected? We limit ourselves to X-ray detections rather than SZ detections because we can probe much lower masses by doing so. Moreover, we have opted to use the combined ROSAT Bright and Faint Source Catalogs as our proxy for an X-ray detected cluster. Because these catalogs do not require the detection of significant *extended* emission — as is required for X-ray cluster catalogs such as NORAS — this allows us to probe a lower detection threshold and to improve our statistics.

We compute the fraction of redMaPPer clusters associated with RASS sources as a function of threshold richness λ and redshift. We bin the redMaPPer clusters in narrow redshift bins of width $\Delta z = \pm 0.025$, starting at $z \in [0.1, 0.15]$ and extending up to $z \in [0.45, 0.5]$. Within each redshift bin, RASS sources are associated with a redMaPPer cluster if the angular separation $\Delta\theta$ is less than 800 kpc at the median redshift of the clusters in the bin. We have found this radius is sufficiently large to capture most true associations while keeping the number of false matches to a minimum. Our chosen aperture corresponds to angles ranging from 2.0 arcmin to 5.4 arcmin depending on the redshift. The probability of a chance association for these apertures is $\approx 10\%$ at $z = 0.1$, falling quickly with redshift to $\lesssim 2\%$ chance associations by redshift $z = 0.35$.

Figure 5 shows the results of this matching exercise. As we would expect, there is some richness λ_{\min} above

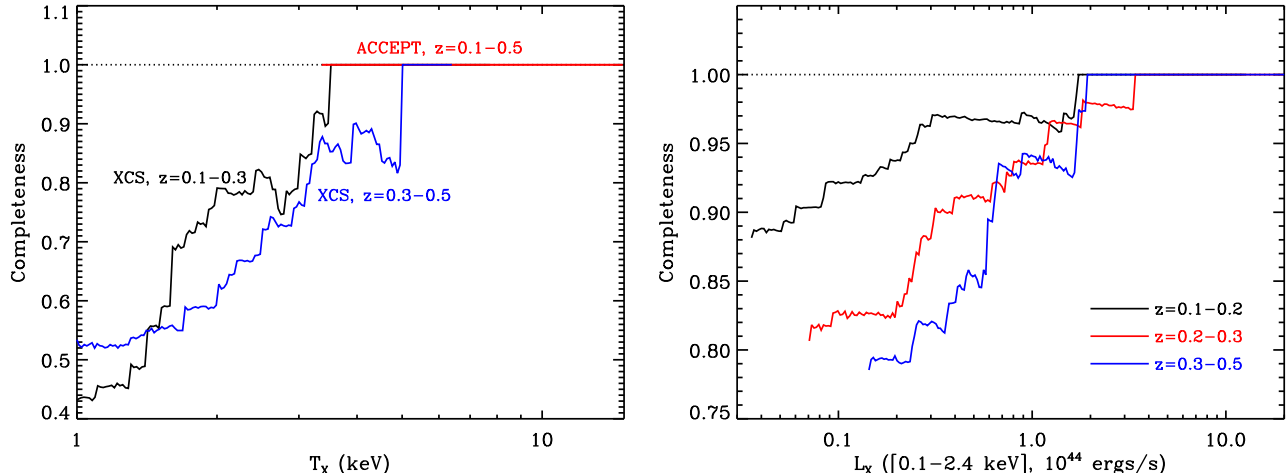


Figure 4. *Left panel:* Fraction of XCS or ACCEPT galaxy clusters detected in redMaPPer, as a function of the temperature threshold T_{\min} , as labeled. At low z , redMaPPer is complete for $T_X \gtrsim 3.5$ keV, with an increasing completeness threshold for $z \geq 0.35$. *Right panel:* Fraction of MCXC galaxy clusters detected in redMaPPer as a function of the luminosity threshold L_X , for three different redshift bins.

which all redMaPPer clusters are X-ray detected, and this richness λ_{\min} increases with redshift. More generally, at fixed richness, the matched fraction decreases with increasing redshift. Note that even for our highest redshift bin, $z \in [0.45, 0.5]$, $\approx 30\%$ of the $\lambda \geq 100$ clusters are X-ray detected.

In our highest redshift bins, there is an obvious flattening of the matched fraction at low richness, a clear indication that those matches are spurious. Interestingly, this flattening occurs at a level that is *higher* than the matching rate for random points quoted above. Thus, the flattening of the curves appears to be impacted by the AGN rate in galaxy clusters. Note that the chance association rate is always much lower than unity, so the high detection rates for rich low redshift clusters are very clearly true physical associations.

Looking at the left panel of Figure 5, there is one redshift bin in particular that looks peculiar, namely the $z \in [0.3, 0.35]$ redshift bin (light green). In this redshift bin, the fraction of X-ray detected clusters drops at $\lambda \gtrsim 110$. Above this richness there are nine clusters, four of which are not detected in X-rays. 3/4 systems that are not X-ray detected exhibit 2 clear distinct galaxy clumps, with each clump hosting a good central candidate. In all 3 cases, the candidate central chosen by redMaPPer is not matched to an X-ray source, but the alternate candidate central is, suggesting these systems are X-ray detected, but grossly miscentered. It is worth noting that in all 3 of these cases, redMaPPer selected the second candidate central as the second most likely central galaxy. Correcting for these three systems makes the $z \in [0.3, 0.35]$ curve much more consistent with the remaining redshift bins, but we have chosen not to apply this correction in Figure 5.

We now investigate whether the evolution of the curves in the left panel of Figure 5 is consistent with the naive expectation that the redMaPPer galaxy clusters form a homogeneous cluster sample with a well defined L_X - λ scaling relation. Specifically, we hypothesize that the only reason why the fraction of galaxy clusters de-

tected in X-rays decreases is due the difficulty of detecting low richness/high redshift clusters in RASS. Let us then define a richness proxy for X-ray flux. Assuming $L_X \propto M^{1.6}$, and $M \propto \lambda$, we arrive at $L_X \propto \lambda^{1.6}$. Ignoring K-corrections and intrinsic evolution in the L_X - λ relation, one expect that the X-ray flux of a galaxy cluster is simply proportional to

$$F_X \propto \lambda^{1.6} D_L(z)^{-2} \quad (3)$$

where $D_L(z)$ is the luminosity distance. Thus, a cluster of richness λ at redshift z has the same X-ray flux as a cluster of richness λ_0 at redshift z_0 where

$$\lambda_0 = \lambda \left(\frac{D_L(z_0)}{D_L(z)} \right)^{2.0/1.6}. \quad (4)$$

Assuming that X-ray detection is limited only by an effective flux threshold, it follows that all the curves in the left panel of Figure 5 should scale onto each other if we scale the x -axis according to Eqn. 4. This is shown in the right panel of Figure 5, where we have set $z_0 = 0.13$ as appropriate for our lowest redshift bin. The good agreement between the various curves demonstrates that the X-ray detection rate is limited primarily by the effective flux limit of RASS.

7. CENTERING

One of the most difficult questions to address within the context of optical cluster finding concerns finding the center of galaxy clusters. While in many cases there is a clear dominant cD galaxy that can be adopted as the cluster center, often times there can be more than one such candidate central. This ambiguity can often be removed with the addition of high resolution X-ray and/or SZ data (e.g., Menanteau et al. 2012; Song et al. 2012; Stott et al. 2012; Mahdavi et al. 2012; von der Linden et al. 2012). Roughly speaking, the correct central galaxy is the largest cD galaxy closest to the X-ray/SZ center. We emphasize, however, that having a good centering proxy is critical for the visual selection

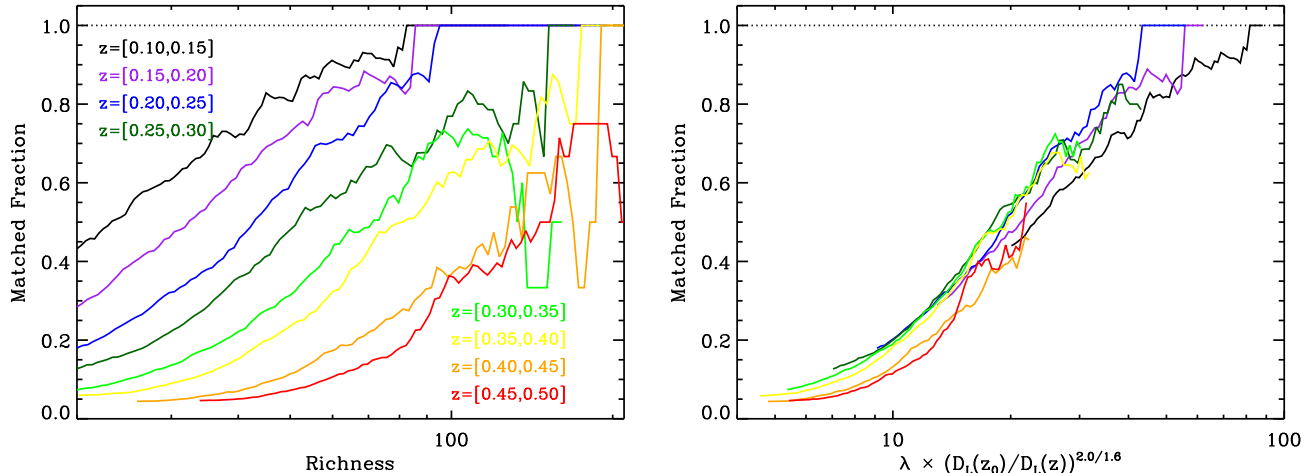


Figure 5. *Left panel:* Fraction of redMaPPer galaxy clusters above a given richness λ matched to a source in the combined ROSAT Bright and Faint Source Catalogs. Each of the curves corresponds to a different redshift bin, as labeled. redMaPPer clusters are matched to ROSAT sources if they fall within an angular aperture corresponding to 800 kpc at the cluster redshift, which ranges from 2.0 arcmin at the highest redshifts to 5.4 arcmin at the lowest redshifts. *Right panel:* As left panel, but the richness is scaled by distance so that the x -axis can be considered a flux proxy. We have ignored K-corrections and any intrinsic evolution in the L_X - λ relation. The fact that the various curves line up demonstrates the X-ray detection rate roughly traces a constant flux limit, as expected.

to be robust. We now investigate how often redMaPPer fails to select the correct central galaxy by evaluating its performance in galaxy clusters with high resolution X-ray data.

We first perform visual inspection of the redMaPPer clusters in the the XCS, ACCEPT, and Mantz galaxy cluster catalogs to determine the correct central galaxy for each cluster. We restrict our analysis to this subsample of galaxy clusters because of the excellent X-ray centroiding that can be achieved with high resolution X-ray instruments. Ultimately, our decision of which galaxy is the correct cluster central is subjective, but proximity to the reported X-ray center was most often the primary criterion used to select the correct central galaxy: we would not attempt this analysis without the X-ray data. We ignore photometric redshift failures in our centering analysis, and we also remove any clusters where the X-ray gas clearly extends beyond the X-ray detector area, a problem that affects some of the XCS systems. Notes on galaxy clusters that merit some discussion are collected in Appendix D.

The left panel in Figure 6 shows the offset distribution between the central galaxies chosen in our visual inspection and the X-ray center reported in each of our reference catalogs. It is obvious that there are two distinct cluster populations contributing to the overall distribution. The first population accounts for $\approx 80\%$ of the X-ray clusters, and is comprised of X-ray clusters where the X-ray centroid and the position of the central galaxy are essentially in perfect agreement ($R \lesssim 50$ kpc). The remaining 20% of the galaxy clusters are merging systems where the gas is significantly offset from the central galaxy, though it's very rare to find systems with an offset larger than $R \approx 300$ kpc.

We turn now to explore how often did redMaPPer choose the correct central galaxy. We combine all three reference catalogs into a single collection of 121 unique X-ray clusters with high resolution X-ray imaging. We find

that the redMaPPer algorithm successfully recovers the central galaxy selected via visual inspection $86.0\% \pm 3.2\%$ of the time. The right panel of Figure 6 shows the distribution of radial offsets between our visually assigned cluster centers and the redMaPPer centers for the 14% of central galaxies that were not correctly selected. The figure legend also indicates the centering success rate for redMaPPer for each of the individual cluster catalogs. The offset distribution can be roughly approximated by a uniform distribution extending out to 0.8 Mpc (dashed green line). Better statistics are required to obtain a more accurate centering model, as there are only 17 clusters in this figure.

8. COMPARISON TO OTHER OPTICAL CATALOGS

We now turn our attention to a comparison of the performance of redMaPPer to that of other photometric cluster finding algorithms that have been applied to SDSS data. The structure of this comparison follows closely the structure of the paper as a whole. As our goal in this section is to compare redMaPPer to other catalogs, as opposed to providing a detailed characterization of all cluster catalogs, our analysis in this section is purposely less thorough than that presented previously for the redMaPPer catalog alone. Specifically, we rely solely on cylindrical matching (see Section 3.1), and we do not take additional steps such as visual inspection of cluster matches to ensure the matchings are appropriate. In addition, we do not take care to find all redshift outliers between each pair of cluster catalogs. These simplifications necessarily have a small quantitative impact on the recovered statistics, but still allow us to fairly compare different cluster catalogs. In particular, in this section we recompute the redMaPPer statistics in exactly the same way as is done for the additional optical catalogs, and refer the reader to the previous sections for the robust statistics of the redMaPPer catalog performance.

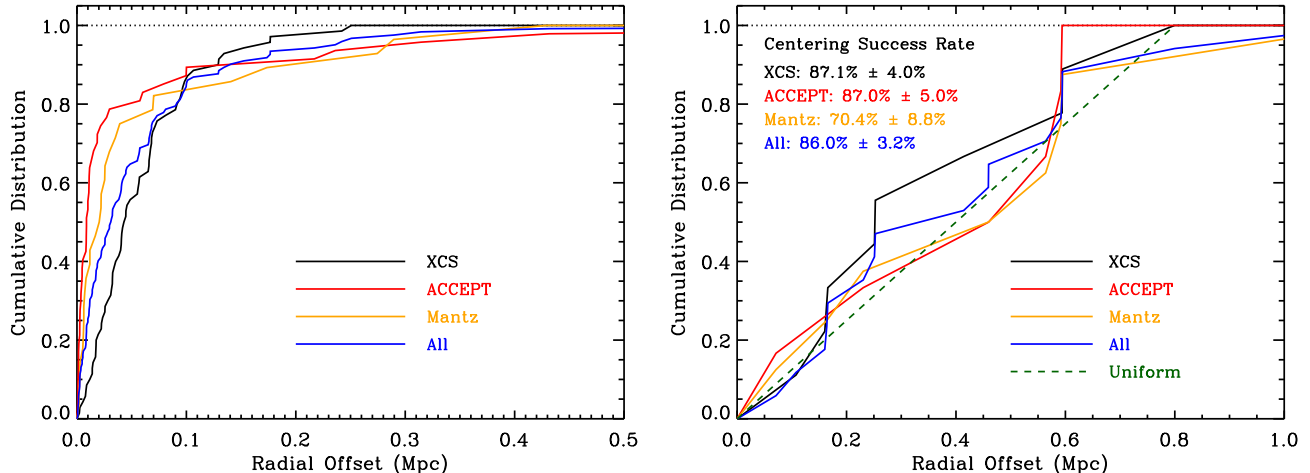


Figure 6. *Left Panel:* Offset distribution between the central galaxy selected by visual inspection and the reported X-ray center for clusters with high resolution X-ray imaging. *Right Panel:* Distribution of radial offsets between our visually assigned cluster centers and the redMaPPer centers for the 14% of central galaxies that were not correctly selected. The redMaPPer centering success rate — i.e., the frequency with which our choice of central galaxy agreed with redMaPPer — is in the figure legend. The dashed dark-green line corresponds to a uniform miscentering model that extends to $R_{\max} = 0.8$ Mpc.

8.1. Comparison Catalogs

We compare the redMaPPer cluster catalog to four additional SDSS optical cluster catalogs.

maxBCG: maxBCG is a red-sequence cluster finding algorithm, where cluster members are selected on the basis of magnitude-independent color cuts (Koester et al. 2007b). Clusters are centered at the brightest cluster member, and the richness is the total number of cluster galaxies above a luminosity threshold $0.4L_*$. The catalog spans 7500 deg^2 , and is limited to the redshift range $z \in [0.1, 0.3]$ (Koester et al. 2007a).

gmBCG: gmBCG is a generalization of maxBCG which does not rely on a pre-parameterized model for the red-sequence of galaxy clusters as a function of redshift (Hao et al. 2010). Instead, the algorithm decomposes the color distribution of galaxies in a given field into two Gaussian components using an error-corrected Gaussian Mixture Model (the “gm” in gmBCG). In fields where there is a galaxy cluster, one of the two Gaussians in the GM decomposition is narrow. Galaxies that contribute to the narrow Gaussian component are identified as cluster members. Clusters are centered at the brightest cluster member, and the richness is the total number of cluster galaxies above a luminosity threshold $0.4L_*$. The catalog spans $\approx 8,200 \text{ deg}^2$ across a redshift range $z \in [0.1, 0.55]$.

AMF: The Adaptive Matched Filter cluster catalog (Szabo et al. 2011) is based on a maximum likelihood algorithm. In this sense, some of the philosophical underpinning of the algorithm are similar to those of redMaPPer, but there are some crucial differences. Specifically, unlike redMaPPer, the AMF algorithm does not rely on red-sequence galaxies. Rather, it utilizes all galaxies, relying on photometric redshift estimates to estimate cluster membership. In addition, the AMF centers galaxy

clusters by maximizing the cluster likelihood over position in the sky, so the center of a galaxy cluster need not coincide with the brightest cluster galaxy. We also note that the AMF algorithm employs spectroscopic data where available in order to assign cluster redshifts. The cluster richness is the total luminosity of the clusters in units of L_* . The catalog spans $\approx 8,400 \text{ deg}^2$ across a redshift range $z \in [0.045, 0.78]$.

Note: Because AMF relies on spectroscopic data where available, we remove clusters with spectroscopic redshifts from the sample when estimating the photometric redshift performance of AMF.

WHL: The WHL cluster catalog (Wen et al. 2012) utilizes galaxy photometric redshifts and a Friends-of-Friends algorithm to group galaxies into distinct clusters. The cluster redshift is estimated using the median photometric cluster redshift of cluster members, and the richness is the total cluster luminosity in units of L_* . The catalog spans $\approx 14,000 \text{ deg}^2$ across a redshift range $z \in [0.05, 0.78]$.

Note: As can be seen in Appendix E, WHL employs a spectroscopic redshift cut such that clusters with $|z_{\text{spec}} - z_{\text{photo}}| \leq 0.055$ are discarded from the cluster catalog. Consequently, we evaluate the redshift performance of the WHL catalog with spectra that are exclusive to DR9, which was not available at the time WHL was published. In addition, we note that WHL removed 3.6% of their clusters after visual inspection. When estimating the fraction of catastrophic photometric redshift outliers we present two results: one for the catalog as published, and the other where we assume that half of the visually removed clusters were redshift outliers.

8.2. Comoving Densities and Data Homogenization

One important difficulty in comparing different cluster catalogs is that one generically expects the performance of all cluster finders to degrade as one moves to lower richness systems. Consequently, a fair comparison must

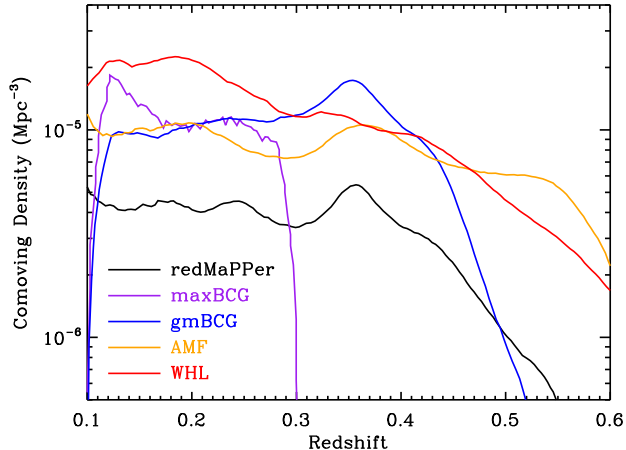


Figure 7. Comoving density as a function of redshift for galaxy clusters in each of the five optical cluster catalogs under consideration. A fair comparison of galaxy clusters requires a uniform selection threshold, which we approximate by demanding that all catalogs have the same redshift-dependent space density as the redMaPPer catalog. This is implemented using a redshift dependent richness cut.

restrict itself to the “same” selection threshold. In practice, each cluster finder uses a different richness and/or selection threshold definition, so there is no unique way of enforcing this condition. Here, we use the comoving density of the galaxy clusters as a proxy for selection threshold.

Figure 7 shows the comoving density of galaxy clusters for each of the five optical cluster catalogs we consider. We see that redMaPPer contains fewer systems per unit volume than any other cluster catalog. As discussed in Paper I, this is by design: we have been purposely conservative in our application of a selection threshold for the SDSS DR8 redMaPPer sample in order to ensure the highest possible data quality.⁴ As the comoving density of the redMaPPer catalog is smaller than all the other cluster catalogs, we apply a redshift-dependent cut on the richness appropriate for each individual catalog such that the resulting cluster sub-samples match the redMaPPer comoving density as a function of redshift.

8.3. Photometric Redshift Performance

We evaluate the photometric redshift performance of the various catalogs by using the spectroscopic redshift catalog from SDSS DR9 (Ahn et al. 2012). Specifically, we compare the photometric redshift estimate of each galaxy cluster to the spectroscopic redshift of either the central galaxy (for catalogs with such a galaxy) or the brightest cluster galaxy (for AMF, which does not specify a central galaxy).

For each sample of galaxy clusters we estimate four statistics: the photometric redshift bias, its standard deviation, its skewness, and the fraction of 4σ photometric redshift outliers. These statistics are estimated as a function of redshift as follows. First, we select all clusters in a bin $z \pm 0.025$. We compute the redshift offset

⁴ For example, were we to relax the redMaPPer selection threshold to $\lambda = 5$, the redMaPPer comoving density would be higher than that of all other cluster catalog by more than a factor of 2.

$\Delta z = z_{\text{spec}} - z_{\text{photo}}$, and then estimate the median redshift and the median absolute deviation of Δz . We then select all galaxy clusters with

$$|\Delta z - \text{med}(\Delta z)| \leq 4 \times 1.4826 \times MAD \quad (5)$$

where MAD is the median absolute deviation. We then use the standard cumulant-based (aka k -statistics) estimator to determine the mean, variance, and skewness of this cluster sub-sample. The scatter σ_z is defined as the square-root of the estimated variance. Finally, we estimate the fraction of $4\sigma_z$ outliers based on the calculated mean and variance. As noted in section 8.1, when evaluating the AMF catalog we restrict our analysis to clusters with photometric redshifts only, and the WHL analysis is restricted to clusters with spectra exclusive to DR9.

Figure 8 collects the four statistics computed above: the photometric redshift bias (top-left), scatter (top-right), skewness (bottom-left), and outlier fraction (bottom-right). The least biased algorithms are redMaPPer and WHL, while redMaPPer and gmBCG have the smallest skewness. redMaPPer outperforms the remaining catalogs in terms of scatter and it has the lowest rate of catastrophic outliers. In short, redMaPPer has the best photometric redshift performance of the five catalogs we considered.

8.4. X-ray Mass Scatter

We now compare the performance of the redMaPPer richness estimator to the richness estimators of other catalogs. To do so, we match each optical catalog to our three high resolution X-ray reference catalogs — XCS, ACCEPT, and Mantz — using cylindrical matching with a radius of $R = 1$ Mpc and a redshift width of $\Delta z_{\text{max}} = 0.05$. For simplicity, we adopt a single redshift bin of $z_{\text{photo}} \in [0.1, 0.5]$. We use the same fitting algorithm as that employed in Section 5 to estimate the scaling relations, including our automated 3σ outlier rejection.

In this context, it is important to note that even if there was no correlation between a given X-ray observable and cluster richness, our test will always recover a finite scatter. For instance, the scatter in M_{gas} at fixed richness cannot be larger than the rms in M_{gas} in the Mantz cluster sample. Consequently, in order to measure the efficacy of a richness estimator as a mass proxy, it is not sufficient to simply measure the scatter in X-ray observables at fixed richness; one must also test whether the observed scatter is significantly smaller than that expected in the absence of any correlation.

We estimate the significance of a sub-random scatter via Monte Carlos. For each optical and X-ray cluster catalog pair (e.g., redMaPPer and XCS), we randomly scramble the richness values among all the matched clusters and remeasure the X-ray observable–richness scatter as above. This procedure is repeated 1000 times to estimate the uncertainty in the scatter for the “random richness” case. This uncertainty is added in quadrature to the error of the recovered scatter for the unshuffled catalog, and then used to evaluate the significance of the difference in scatter between the original and richness-shuffled catalogs.

As a final test the efficacy of the various cluster richness estimators, we have also estimated the Pearson correla-

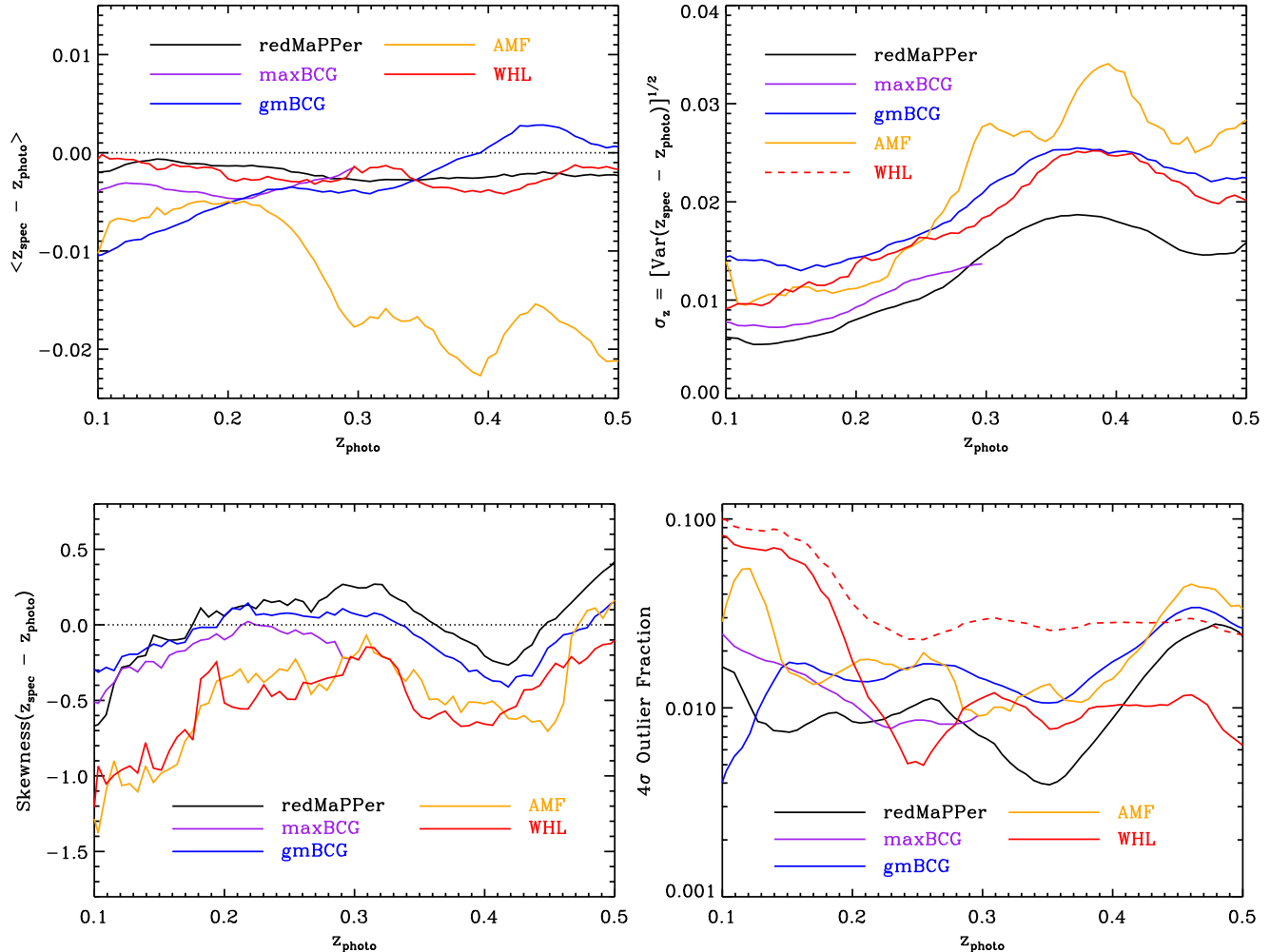


Figure 8. *Top-Left:* Photometric redshift bias as a function of redshift for each of the five optical catalogs under consideration. *Top-Right:* Photometric redshift scatter. *Bottom-Left:* Skewness of the photometric redshift offset distribution. *Bottom-right:* Fraction of 4σ redshift outliers. The dashed red-line assumes half of the 3.6% catastrophic failures in the WHL catalog that were removed from visual inspection were redshift outliers (see text).

tion coefficient for each of the cluster samples, limiting ourselves to clusters that are not flagged as outliers by our automated outlier rejection algorithm.

Our results are summarized in Table 3. We see that in all cases the redMaPPer richness estimator results in the smallest scatters. Furthermore, the reduction in scatter relative to the shuffled-richness catalog is also most significant in the case of redMaPPer catalog. In fact, redMaPPer is the only catalog that shows consistent evidence ($\geq 3\sigma$) that the X-ray observable–richness scatter is significantly lower than that of a richness-shuffled catalog. Similarly, redMaPPer always exhibits the largest correlation coefficients across all X-ray catalogs. In short, the redMaPPer richness is clearly better correlated with X-ray temperature and M_{gas} than the richness measures of the remaining optical catalogs.

8.5. Completeness

To estimate the X-ray completeness of a given optical catalog, we must first determine whether any given X-ray cluster falls within the footprint of the optical clus-

ter catalog in question. Unfortunately, we do not have the detection masks for each individual cluster catalog, so we must resort to an approximate method to make this decision. We assume that X-ray clusters that fall within 40 arcmin of any optical cluster are within the optical footprint of the corresponding cluster catalog. The choice of this aperture is motivated by the angular density of redMaPPer clusters, which corresponds to an average of ~ 1 cluster per circle of radius 20 arcmin. The motivation for setting this angular scale based on redMaPPer systems is motivated by the fact that the redMaPPer catalog is the one with the lowest density of galaxy clusters. Of course, our method for determining which clusters fall insider or outside the various masks is not ideal, but it does have the benefit of treating the footprint of all the optical catalogs in the same way.

Having established which X-ray clusters fall within the footprint of a given optical cluster catalog, we select all X-ray systems with $z \in [0.1, 0.5]$, except for when comparing with the maxBCG catalog, in which case we restrict ourselves to the redshift range $z \in [0.1, 0.3]$. We

Table 3
Comparison of the efficacy of different richness measures as mass tracers

Catalog	XCS			ACCEPT			Mantz		
	Scatter	Sig.	r	Scatter	Sig.	r	Scatter	Sig.	r
redMaPPer	0.244 ± 0.035	3.0σ	0.61	0.200 ± 0.021	4.1σ	0.67	0.201 ± 0.033	6.4σ	0.83
maxBCG	0.430 ± 0.132	0.7σ	0.40	0.326 ± 0.122	1.6σ	0.54	0.363 ± 0.064	1.0σ	0.43
gmBCG	0.275 ± 0.060	1.5σ	0.56	0.203 ± 0.024	3.5σ	0.66	0.357 ± 0.052	2.3σ	0.63
AMF	0.273 ± 0.042	1.8σ	0.53	0.222 ± 0.037	1.4σ	0.53	0.227 ± 0.094	2.7σ	0.79
WHL	0.305 ± 0.034	2.3σ	0.52	0.233 ± 0.020	1.3σ	0.39	0.335 ± 0.058	3.0σ	0.70

Note. — The XCS/ACCEPT scatter is the scatter in T_X at fixed richness, while Mantz scatter is the scatter in M_{gas} at fixed richness. In all cases, "Sig." is the significance of the reduction in scatter relative to the case where the cluster richnesses are randomly shuffled, while r is the Pearson correlation coefficient.

then use the cylindrical matching method of Section 3.1 (with radius 1 Mpc and $\Delta z_{\text{max}} = 0.05$) to obtain a set of exclusive two-way matches. As in other sections, when evaluating the completeness we enforce density matching with the redMaPPer catalog.

Figure 9 summarizes our completeness results. When computing the completeness as a function of T_X (left panel), we compute the completeness function using the XCS and ACCEPT catalogs, and take the average of the two completeness functions. When computing the completeness as a function of L_X (right panel), the luminosities are estimated using the MCXC catalog. We observe that in both cases the redMaPPer catalog is the most complete. We emphasize that while this analysis has the virtue of treating all optical cluster catalogs identically, the resulting completeness functions are underestimated due to the approximate handling of the mask, the bad redshifts in the X-ray catalogs, and the lack of optical inspection to adjust spurious matches. For the true redMaPPer completeness function, see Figure 4.

8.6. Purity

Following Section 6.2, we estimate the purity of each photometric cluster catalog by matching it to the ROSAT Bright and Faint Source Catalogs. We use four redshift bins from $z = 0.1$ to $z = 0.5$ in steps of $\Delta z = 0.1$. X-ray sources are considered matched to galaxy clusters if they are within an angular separation of 1 Mpc at the median redshift of the appropriate redshift bin.

Our results are summarized in Figure 10. Because the X-ray detection rate is a function of richness, we must properly account for the fact that the different cluster catalogs all have different richness definitions. Therefore, we present our results as a function of *density* rather than richness. Each panel corresponds to a different redshift bin, and each color corresponds to a different cluster catalog, as labeled. We see that at low redshifts, the fraction of redMaPPer clusters that is X-ray detected is clearly higher than that of the remaining cluster catalogs. By the $z \in [0.3, 0.4]$ redshift bin — the AMF and redMaPPer algorithms have essentially identical performance, and at $z \in [0.4, 0.5]$, the redMaPPer, AMF, and WHL catalogs all have comparable X-ray detection rates.

These results clearly indicate that photometric noise and survey depth play a critical role in the performance of cluster finding algorithms. When the data is such that the photometric noise is low, redMaPPer clearly outperforms the remaining cluster finding algorithms. As the cluster galaxies approach the magnitude limit of the sur-

vey, however, the difference in performance between the various cluster catalogs becomes less pronounced. For future surveys like the DES or LSST, the redshift at which the photometric limit becomes comparable to the magnitude of the cluster galaxies being selected is expected to be $z \approx 0.9$ and $z \approx 1.5$ respectively.

8.7. Centering

As in our centering offset analysis of the redMaPPer catalog in Section 7, we match each of the photometric catalogs under consideration to an X-ray catalog comprised of all unique galaxy clusters in the combined XCS, ACCEPT, and Mantz cluster catalogs. For each matched cluster, we compute the radial offset between the reported X-ray center and the reported optical center, from which we then compute the cumulative distribution function.

Our results are summarized in Figure 11. We see that the redMaPPer, maxBCG, gmBCG, and WHL cluster catalogs have essentially identical centering distributions, while AMF performs significantly worse. Interestingly, the AMF algorithm is the only algorithm that does not rely on galaxy locations to define the cluster center. Rather, their cluster centers are based on maximizing a likelihood in the plane of the sky. Evidently, the prior that the cluster center falls on a cluster galaxy is highly informative, and leads to significant improvement in the centering performance.

Just as interestingly, the redMaPPer, maxBCG, gmBCG, and WHL algorithms vary widely in the sophistication of their centering algorithms, ranging from as simple as “pick the brightest member”, as done in WHL and maxBCG, to the iterative self-training algorithm of redMaPPer (see Paper I). On the one hand, this might suggest that the redMaPPer algorithm is unnecessarily complicated. On the other hand, our sophisticated algorithm has an important advantage relative to the remaining cluster finders: redMaPPer is the only algorithm capable of estimating centering probabilities for each potential central galaxy. That said, we note that a detailed quantitative test of whether the redMaPPer centering probabilities are indeed correctly estimated has not yet been performed, a problem that we will return in a future work. For now, we will simply state that our internal tests have produced good evidence that the centering probability is well correlated with the likelihood of cluster being correctly centered, i.e. clusters with low centering probability are more often incorrectly centered. However, whether the centering probabilities are quanti-

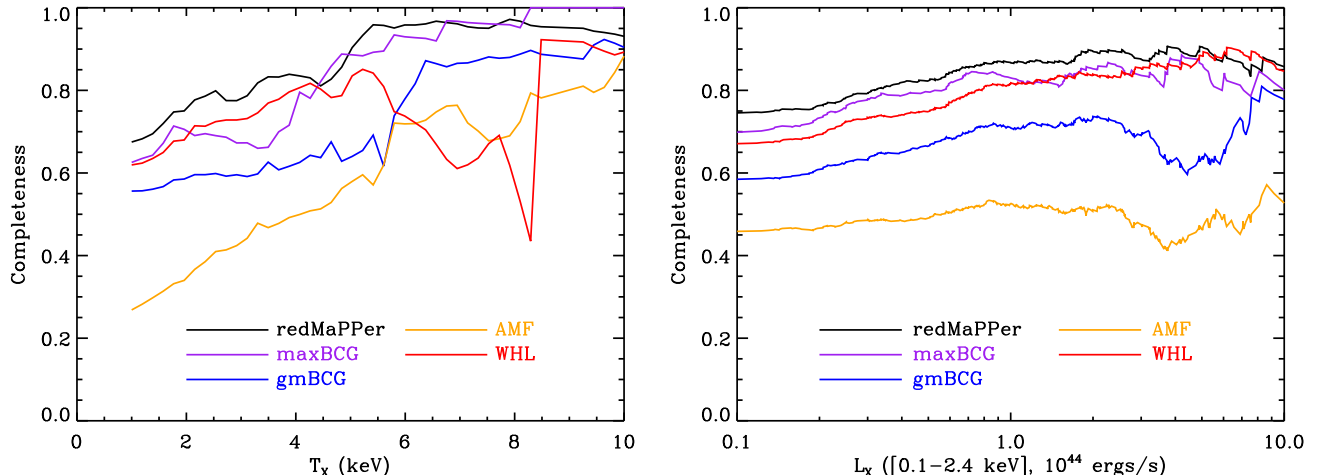


Figure 9. Fraction of X-ray clusters detected by each of the optical catalogs, as a function of X-ray temperature (left) or X-ray luminosity (right) for all clusters with $z \in [0.1, 0.5]$ ($z \in [0.1, 0.3]$ for maxBCG). We caution this plot uses only an approximate treatment to determine which X-ray clusters fall within the optical masks of each catalog, which necessarily leads to an underestimate of the completeness. However, the treatment of the optical mask is the same across all catalogs (see text).

tatively correct remains to be determined.

9. SUMMARY AND CONCLUSIONS:

We have performed an extensive quality test of the performance of the SDSS redMaPPer cluster catalog by comparing it against several X-ray and SZ cluster catalogs. We find that the redMaPPer redshifts are nearly unbiased, with biases falling at the 0.005 level or below. In addition, our photometric redshifts exhibit remarkably low scatter, as low as ≈ 0.006 at low redshift, but increasing with redshift due to the increase in photometric noise in the data. Moreover, the scatter in redshift is nearly symmetrical, and has a very low ($\approx 1\%$) catastrophic failure rate. In this context, it is important to emphasize that the word “catastrophic” here means that the true cluster redshift is more than 4σ away from our photometric redshift estimate. Because our photo- z scatter is so low, clusters with $|z_{\text{spec}} - z_{\text{photo}}|$ as low as ≈ 0.025 can be considered catastrophic failures. We note too that in addition to providing a simple photometric cluster redshift, the redMaPPer catalog includes an estimate of the full redshift probability distribution $P(z)$ for every galaxy cluster (see Paper I).

We have also tested the performance of our richness estimator λ (see also Roza et al. 2009b; Rykoff et al. 2012) using our reference X-ray catalogs. In particular, using the XCS and ACCEPT cluster catalogs we have estimated the scatter in X-ray temperature at fixed richness, and converted it to an equivalent scatter in mass at fixed richness. Both data sets are consistent with each other, and the combined analysis suggest a scatter in mass at fixed richness of 26%. We have further verified this analysis by utilizing the Mantz cluster sample to measure the scatter in the $M_{\text{gas}}-\lambda$ relation, from which we are able to recover an equivalent mass scatter of 21%. Given the systematic uncertainties associated with our measurements — most importantly the fact that the selection function of the clusters with combined optical and X-ray data is not well constrained — we estimate that a reasonable range for the scatter in mass at fixed richness

for the redMaPPer clusters is $25\% \pm 5\%$. Interestingly, this scatter may well be comparable to the estimated scatter from SZ mass proxies in current SZ surveys such as ACT and SPT (Benson et al. 2013; Hasselfield et al. 2013), and better than what has been achieved with Planck so far using SZ data only (Planck Collaboration 2011b). We hasten to add, however, that we do expect significant improvement in future Planck data releases.

In this context, it is also worth emphasizing that we did find one clear cluster outlier in our analysis — cluster 400D J1416.4+4446 — whose richness was grossly over-estimated due to projection effects. The existence of this one outlier suggest that $\approx 1\%$ of our galaxy clusters suffer from projection effects. This failure rate is somewhat lower than what was estimated in Paper I, where we found that up to $\approx 5\%$ of the galaxy clusters can be severely affected by projection effects, particularly at the rich end. The lower failure rate measured in this work is likely to be related to our reliance on external X-ray catalog for the majority of our tests, as X-ray selected sub-samples of the redMaPPer clusters are expected to be more robust to projection effects.

We have also explored the completeness of the redMaPPer cluster catalog as a function of X-ray luminosity, temperature, gas mass, and SZ detectability. redMaPPer detects all galaxy clusters in the Mantz sample, ACCEPT sample, and Planck ESZ sample. At low ($z \lesssim 0.35$) redshifts, where the redMaPPer catalog is volume limited, the catalog is 100% complete at $T_X \gtrsim 3.5$ keV, and above a luminosity threshold of $L_X \gtrsim 2 \times 10^{44}$ ergs/s. Because of the large scatter ($\approx 60\% - 70\%$) in the relation between X-ray luminosity and cluster richness, the decrease in completeness with decreasing luminosity is very modest; at low redshifts, the catalog remains $\approx 90\%$ complete all the way down to $L_X \approx 10^{43}$ ergs/s.

In addition, we have estimated the fraction of redMaPPer galaxy clusters that are X-ray detected by cross-matching our catalog with the ROSAT Bright and Faint Source Catalogs. As expected, all rich, low redshift clus-

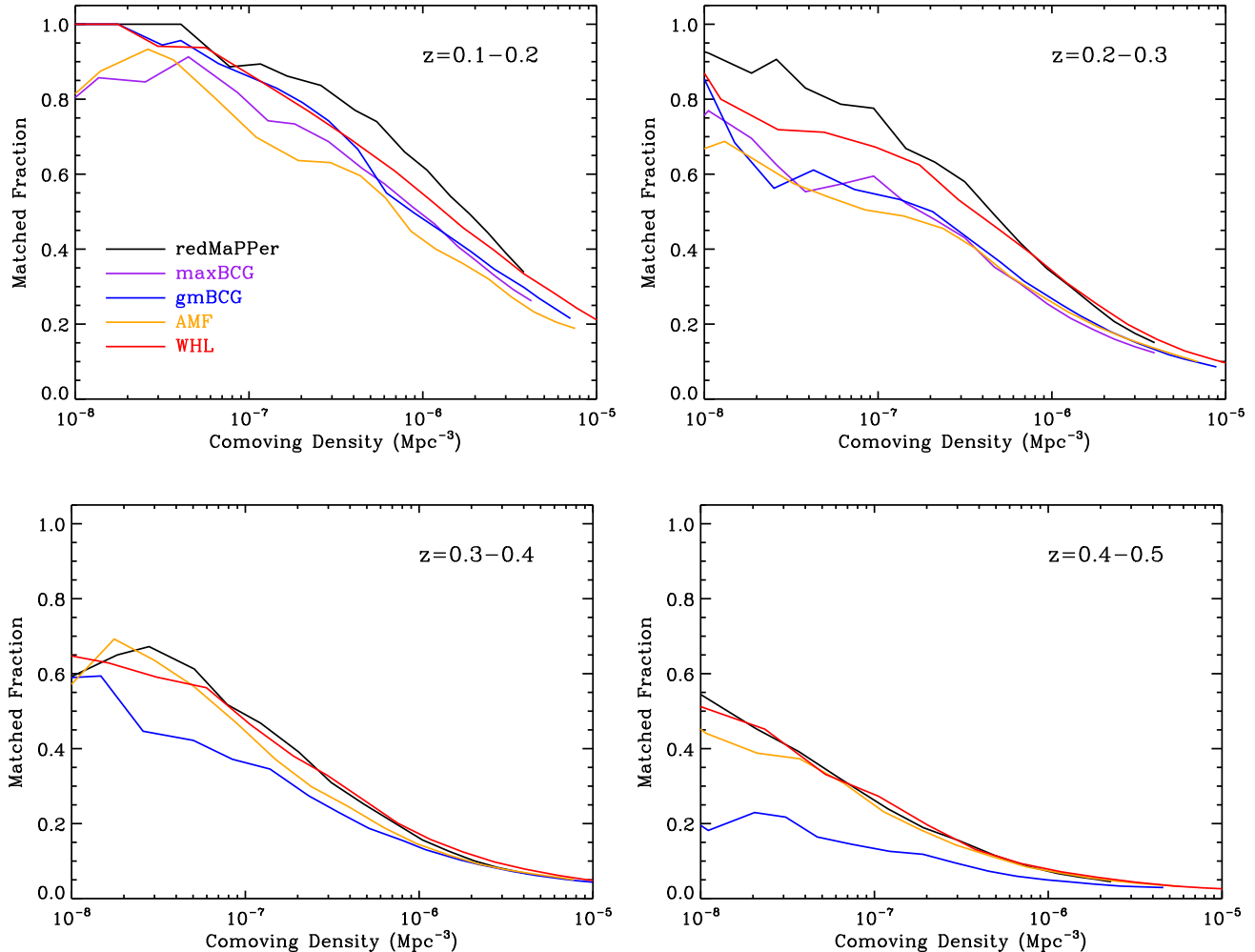


Figure 10. Fraction of optically selected galaxy clusters detected as X-ray sources in the ROSAT Bright or Faint Source Catalogs as a function of redshift, as labeled. X-ray sources are matched to clusters if they are within an angular separation θ such that θ subtends 1 Mpc at the median cluster redshift within each bin.

ters are X-ray detected, with the detection fraction decreases with increasing redshift and/or decreasing richness. We have verified that this decrease in the detection fraction is primarily — and most likely exclusively — driven by the decrease in the expected X-ray flux of the galaxy clusters with decreasing richness and increasing redshift. That is, we see no evidence of a large population of intrinsically X-ray dark clusters. Of course, as noted above, we do have clear evidence for a population of galaxy clusters that suffers from projection effects, comprising $\approx 1\%$ of the cluster sample.

We have further measured the miscentering rate of the redMaPPer galaxy clusters by visually inspecting 121 galaxy clusters with high resolution X-ray data. Based on our visual inspection and the reported X-ray centers, we identified the correct central galaxy for each of these clusters, and compared it to the galaxy that was selected by the redMaPPer cluster catalog, finding that $\approx 86\%$ of the redMaPPer galaxy cluster are correctly centered.

Finally, we also performed a “quick-and-dirty” version of all of the above analyses on all photometric cluster catalogs in the SDSS published to date. Our goal here is

not to characterize in detail the performance of each of these cluster catalogs, but rather to provide a meaningful comparison among them. Note in particular that when performing these comparisons, the redMaPPer catalog is treated in the exact same way as the remaining cluster catalogs.

As the result of this comparison, we find that the redMaPPer catalog has a higher completeness than that of any other cluster catalog. As for purity, we find that at low redshift the redMaPPer algorithm has a higher X-ray detection rate than that of any other catalog. However, as the survey depth becomes comparable to the magnitude of the bulk of the galaxy population of galaxy clusters, the differences between the various algorithms decrease. At $z \in [0.3, 0.4]$, the redMaPPer and AMF algorithm have comparable X-ray detection rates, and at $z \in [0.4, 0.5]$, the WHL algorithm also reaches an X-ray detection rate comparable to that of redMaPPer and AMF. We note that in the Dark Energy Survey, the transition point at which the survey depth becomes comparable to the magnitude of the cluster galaxies is $z \approx 0.9$.

Turning to the redshift performance comparison, the

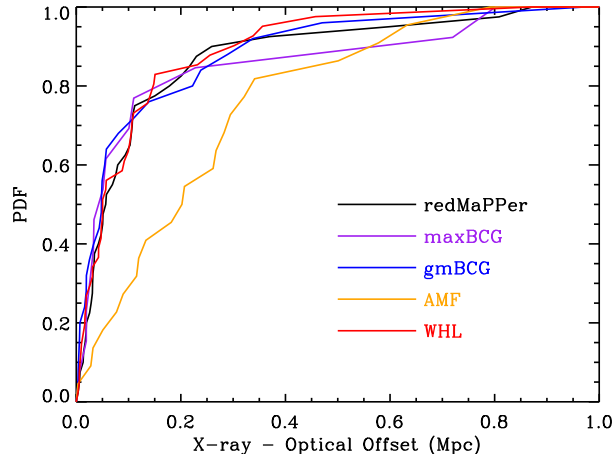


Figure 11. Distribution of the radial offset between the X-ray and optical centers for matched galaxy clusters in each of the optical catalogs under consideration, as labeled. The X-ray sample is comprised of all unique X-ray clusters from the combined XCS, ACCEPT, and Mantz cluster samples. All the catalogs have very similar centering performance characteristics except for AMF, which is the only catalog not to explicitly select a bright galaxy as the center.

redMaPPer photometric redshifts are the least biased, with the WHL redshifts — themselves based on the DR8 photometric redshifts — being equally unbiased. The redMaPPer redshifts clearly exhibit the lowest scatter amongst all catalogs, and, along with the gmBCG redshift, they exhibit the least amount of skewness. The catastrophic failure rate of the redMaPPer redshifts is the lowest amongst the SDSS clusters catalogs.

We also compared the performance of the redMaPPer richness estimator to that of the various other cluster catalogs, both via the T_X -richness scaling relations, and via the M_{gas} -richness scaling relations. The redMaPPer catalog consistently exhibited the lowest scatter on all relations. Moreover, the redMaPPer catalog is the only one to consistently show evidence ($\geq 3\sigma$) for the recovered scatter being lower than that estimated when the richnesses are randomly shuffled amongst all clusters.

Finally, turning to cluster centering, we found that the centering algorithm in redMaPPer performs as well as — i.e., neither better nor worse — the remaining catalogs. The only exception was the AMF catalog, which performed worse. Since AMF is the only catalog that did not choose to center the galaxy clusters by identifying a central galaxy, it is clear that the prior that galaxy clusters should be centered on bright cluster galaxies is highly informative, and improves the overall performance of a cluster finder. We also emphasize that while the remaining cluster catalogs all had equivalent centering performances, the redMaPPer catalog is unique in that the algorithm estimates the probability that the chosen central galaxy is correct, and also provides 4 additional candidate central galaxies along with their corresponding probabilities. Our hope is that cluster miscentering can be robustly treated using these estimated probabilities, but we postpone the development of a statistical framework that exploits this information to a future work. For now, we simply note that redMaPPer is the only algo-

rithm for which such a framework can be developed.

As an important caveat to our results, we wish to emphasize that the results of our optical cluster comparison presented in this work reflect the reality of the various cluster finding algorithms as implemented in the SDSS, with the data that was available at the time. In particular, it is worth keeping in mind that the performance of photometric redshift cluster finders such as AMF and WHL will depend not only on the cluster finding algorithm itself, but also on the quality of the redshifts employed in the construction of the photo- z estimates. For instance, AMF relied on SDSS DR6 data with photo- z estimates from Oyaizu et al. (2008), while WHL relied on SDSS DR8 photo- z s. Given that there has been a great deal of improvement between the DR6 photo- z s from Oyaizu et al. (2008) and the DR8 photo- z s — in large part due to increasingly large training samples for photo- z machine learning methods, with current samples reaching over 850,000 galaxies⁵ — it is reasonable to expect the performance of AMF to improve if run using DR8 photo- z s. That said, we believe that the fact that the redMaPPer performance is in no way limited by the performance of galaxy photo- z measurements is still clearly a valuable feature. Moreover, while redMaPPer does require spectroscopic training samples, just as photo- z measurements do, it is important to emphasize that, as demonstrated in Paper I, redMaPPer can deliver photometric redshift quality using a spectroscopic training sample comprised of only the 400 brightest cluster galaxies in SDSS (sampled over the full redshift range, see paper I for details).

The excellent performance of redMaPPer in the Sloan Digital Sky Survey provides strong evidence that upcoming photometric surveys like the Dark Energy Survey and LSST will be capable of producing very large, high quality cluster samples. Moreover, the excellent quality of the photometric redshifts, the low rate of catastrophic redshift failures and projection effects, and the low scatter in the optical mass proxy, all suggest that the quality of photometric cluster catalogs should easily suffice from the point of view of precision cosmology. In particular, a $\approx 1\% - 2\%$ catastrophic failure rates on these algorithms is comparable to the expected precision of the cluster mass estimates that can be achieved in surveys like the Dark Energy Survey (e.g. Oguri & Takada 2011; Weinberg et al. 2012), suggesting that optical detection systematics are not likely to be a dominant source of errors in near-future photometric surveys. The most important exception remains cluster centering: with only 85% of the redMaPPer galaxy clusters being correctly centered, there is a clear need for a robust statistical framework with which to address this problem, a question that we will return to in future work.

The authors would like to thank M. Donahue for her help with the ACCEPT cluster catalog, and Alexis Finoguenov and Marguerite Pierre for useful comments on an earlier draft of this paper. This work was supported in part by the U.S. Department of Energy contract to SLAC no. DE-AC02-76SF00515.

Funding for SDSS-III has been provided by the Alfred

⁵ <http://www.sdss3.org/dr9/algorithms/photo-z.php>

P. Sloan Foundation, the Participating Institutions, the National Science Foundation, and the U.S. Department of Energy Office of Science. The SDSS-III web site is <http://www.sdss3.org/>.

SDSS-III is managed by the Astrophysical Research Consortium for the Participating Institutions of the SDSS-III Collaboration including the University of Arizona, the Brazilian Participation Group, Brookhaven National Laboratory, University of Cambridge, Carnegie Mellon University, University of Florida, the French Participation Group, the German Participation Group, Harvard University, the Instituto de Astrofísica de Canarias, the Michigan State/Notre Dame/JINA Participation Group, Johns Hopkins University, Lawrence Berkeley National Laboratory, Max Planck Institute for Astrophysics, Max Planck Institute for Extraterrestrial Physics, New Mexico State University, New York University, Ohio State University, Pennsylvania State University, University of Portsmouth, Princeton University, the Spanish Participation Group, University of Tokyo, University of Utah, Vanderbilt University, University of Virginia, University of Washington, and Yale University.

REFERENCES

- Abell, G. O. 1958, *ApJS*, 3, 211
 Abell, G. O. et al. 1989, *ApJS*, 70, 1
 Ahn, C. P. et al. 2012, *ApJS*, 203, 21
 Aihara, H. et al. 2011, *ApJS*, 193, 29
 AMI Consortium. 2011, *MNRAS*, 414, L75
 Andreon, S. 2012, *A&A*, 548, A83
 Andreon, S. & Moretti, A. 2011, *A&A*, 536, A37
 Angulo, R. E. et al. 2012, *ArXiv:1203.3216*
 Annis, J. et al. 1999, in *Bulletin of the American Astronomical Society*, Vol. 31, American Astronomical Society Meeting Abstracts, 1391
 Bahcall, N. A. et al. 2003, *ApJS*, 148, 243
 Balogh, M. L. et al. 2011, *MNRAS*, 412, 947
 Barrena, R. et al. 2007, *A&A*, 469, 861
 Benson, B. A. et al. 2013, *ApJ*, 763, 147
 Biviano, A. 2000, in *Constructing the Universe with Clusters of Galaxies*
 Böhringer, H. et al. 2000, *ApJS*, 129, 435
 —. 2004, *A&A*, 425, 367
 Burenin, R. A. et al. 2007, *ApJS*, 172, 561
 Cavagnolo, K. W. et al. 2009, *ApJS*, 182, 12
 Clerc, N. et al. 2012, *MNRAS*, 423, 3561
 Cohn, J. D. et al. 2007, *MNRAS*, 382, 1738
 Cruddace, R., Voges, W., Böhringer, H., Collins, C. A., Romer, A. K., MacGillivray, H., Yentis, D., Schuecker, P., Ebeling, H., & De Grandi, S. 2002, *ApJS*, 140, 239
 Dai, X., Bregman, J. N., Kochanek, C. S., & Rasia, E. 2010, *ApJ*, 719, 119
 David, L. P. & Kempner, J. 2004, *ApJ*, 613, 831
 Dawson, K. S. et al. 2013, *AJ*, 145, 10
 Donahue, M. et al. 2001, *ApJ*, 552, L93
 Durret, F. et al. 2011a, *A&A*, 535, A65
 —. 2011b, *A&A*, 529, A38
 Ebeling, H. et al. 1998, *MNRAS*, 301, 881
 —. 2001, *ApJ*, 553, 668
 —. 2002, *ApJ*, 580, 774
 —. 2010, *MNRAS*, 407, 83
 Eisenstein, D. J. et al. 2001, *AJ*, 122, 2267
 Frenk, C. S. et al. 1990, *ApJ*, 351, 10
 Gal, R. R. et al. 2009, *AJ*, 137, 2981
 Gioia, I. M. et al. 1990, *ApJS*, 72, 567
 Gladders, M. D. & Yee, H. K. C. 2000, *AJ*, 120, 2148
 Gladders, M. D. et al. 2007, *ApJ*, 655, 128
 Haines, C. P. et al. 2009, *MNRAS*, 396, 1297
 Hao, J. et al. 2010, *ApJS*, 191, 254
 Hasselfield, M. et al. 2013, *ArXiv:1301.0816*
 Henry, J. P. et al. 2006, *ApJS*, 162, 304
 —. 2009, *ApJ*, 691, 1307
 Horner, D. J. et al. 2008, *ApJS*, 176, 374
 Israel, H. et al. 2012, *A&A*, 546, A79
 Kaiser, N. et al. 2002, in *Society of Photo-Optical Instrumentation Engineers (SPIE) Conference Series*, Vol. 4836, Society of Photo-Optical Instrumentation Engineers (SPIE) Conference Series, ed. J. A. Tyson & S. Wolff, 154–164
 Kelly, B. C. 2007, *ApJ*, 665, 1489
 Kepner, J. et al. 1999, *ApJ*, 517, 78
 Kocevski, D. D. et al. 2007, *ApJ*, 662, 224
 Koester, B. et al. 2007a, *ApJ*, 660, 239
 Koester, B. P. et al. 2007b, *ApJ*, 660, 221
 Lopes, P. A. A. et al. 2009, *MNRAS*, 399, 2201
 LSST Dark Energy Science Collaboration. 2012, *ArXiv e-prints*
 Lucey, J. R. 1983, *MNRAS*, 204, 33
 Mahdavi, A. et al. 2012, *ArXiv:1210.3689*
 Mantz, A. et al. 2010a, *MNRAS*, 406, 1759
 —. 2010b, *MNRAS*, 406, 1773
 Mazzotta, P. et al. 2004, *MNRAS*, 354, 10
 Mehrtens, N. et al. 2012, *MNRAS*, 423, 1024
 Menanteau, F. et al. 2012, *ArXiv:1210.4048*
 Milkeraitis, M. et al. 2010, *MNRAS*, 406, 673
 Mullis, C. R. et al. 2003, *ApJ*, 594, 154
 Noh, Y. & Cohn, J. D. 2011, *MNRAS*, 158
 Oguri, M. & Takada, M. 2011, *Phys. Rev. D*, 83, 023008
 Okabe, N. & Umetsu, K. 2008, *PASJ*, 60, 345
 Okabe, N. et al. 2010, *PASJ*, 62, 811
 Oyaizu, H. et al. 2008, *ApJ*, 674, 768
 Piffaretti, R. et al. 2011, *A&A*, 534, A109
 Planck Collaboration. 2011a, *A&A*, 536, A8
 —. 2011b, *A&A*, 536, A11
 —. 2011c, *A&A*, 536, A12
 Pratt, G. W. et al. 2009, *A&A*, 498, 361
 Rasmussen, J. et al. 2006, *MNRAS*, 373, 653
 Romer, A. K. et al. 2000, *ApJS*, 126, 209
 Rozo, E., Vikhlinin, A., & More, S. 2012a, *ArXiv:1202.2150*
 Rozo, E. et al. 2009a, *ApJ*, 699, 768
 —. 2009b, *ApJ*, 703, 601
 —. 2010, *ApJ*, 708, 645
 —. 2011, *ApJ*, 740, 53
 —. 2012b, *ArXiv:1204.6292*
 —. 2012c, *ArXiv:1204.6305*
 Rykoff, E. S. et al. 2012, *ApJ*, 746, 178
 Soares-Santos, M. et al. 2011, *ApJ*, 727, 45
 Song, J. et al. 2012, *ApJ*, 747, 58
 Stott, J. P. et al. 2012, *MNRAS*, 422, 2213
 Strauss, M. A. et al. 2002, *AJ*, 124, 1810
 Szabo, T. et al. 2011, *ApJ*, 736, 21
 Thanjavur, K. et al. 2009, *ApJ*, 706, 571
 The DES Collaboration. 2005, *ArXiv:0510346*
 van Breukelen, C. & Clewley, L. 2009, *MNRAS*, 395, 1845
 van Haarlem, M. P. et al. 1997, *MNRAS*, 287, 817
 Vikhlinin, A. et al. 1998, *ApJ*, 502, 558
 —. 2009a, *ApJ*, 692, 1033
 —. 2009b, *ApJ*, 692, 1060
 Voges, W. et al. 1999, *A&A*, 349, 389
 —. 2000, *VizieR Online Data Catalog*, 9029, 0
 von der Linden, A. et al. 2012, *ArXiv:1208.0597*
 Wang, L. et al. 2011, *ArXiv e-prints*
 Weinberg, D. H. et al. 2012, *ArXiv:1201.2434*
 Wen, Z. L. et al. 2012, *ApJS*, 199, 34
 White, M. et al. 2010, *MNRAS*, 408, 1818
 Zwicky, F. et al. 1968, *Catalogue of galaxies and of clusters of galaxies (Pasadena: California Institute of Technology (CIT), 1961-1968)*

APPENDIX

A. CLUSTERS WHERE MATCHINGS DIFFERED

Below is the complete list of galaxy clusters where the cylindrical and membership matching algorithms differed.

XCS:

XCS J1310.9+5720: No cylindrical match. There are two clear galaxy clumps at this redshift, with the XCS cluster corresponding to the northern component. In redMaPPer, the southern component is richer, so it is this southern

component that was matched to the XCS cluster. However, the northern component is also detected, and is the obvious correct match.

XCS J0920.8+3028: Cylindrical and membership matches differ. This cluster is at the eastern component of Abell 781. redMaPPer identifies both the eastern and western component, but the membership matching matches the XCS system to the western component because it is richer.

XCS J0943.5+1639: Cylindrical and membership matches differ. The membership match is correct. The cylindrical match for this clusters is a foreground cluster at $z = 0.18$ (compared to $z = 0.25$).

XCS J2337.9+2711: No cylindrical match. Membership match is clearly correct.

XCS J0943.9+1641: No cylindrical match. Membership map is a larger cluster due NW which is not included in the XCS catalog. The correct match is found by redMaPPer algorithm, but with a richness that falls below our selection threshold in Paper I.

XCS J1256.8+2548: No cylindrical match. Membership match incorrect: correct match is a redMaPPer cluster that falls below our selection threshold.

XCS J0840.7+3830: No membership match. Correct match is clearly a redMaPPer cluster that falls below our selection threshold.

MCXC:

MCXC J1326.2+1230: No cylindrical match. This is a small satellite cluster of the much larger system Abell 1735, and does not pass the redMaPPer selection threshold.

MCXC J1230.7+3439: This is an interesting system. The X-ray location is close to a cD galaxy, which falls roughly in the middle of 2 redMaPPer clusters at the same redshift. The least rich of these 2 redMaPPer clusters is subject to masking from the richer system, which is the membership match of the X-ray system. In this sense, the membership match is clearly correct, but it may be subject to miscentering. Unambiguous evidence for miscentering would require high resolution X-ray imaging.

MCXC J1227.1+1951: No cylindrical match. Membership match is clearly correct.

MCXC J0751.4+1730: No cylindrical match. The photometry around this region is clearly compromised. We set this cluster to unmatched to reflect the photometric failure, even though technically a cluster was found.

MCXC J1415.2-0030: No cylindrical match. This cluster is Abell 1882, which has two clear components. redMaPPer is centered on the NW component, whereas the MCXC system corresponds to the SE component. The SE component appears to be the most massive one based on the X-ray data, suggesting the cluster is catastrophically miscentered in redMaPPer. The membership matching association is clearly correct.

MCXC J1311.8+3227: No cylindrical match. Membership match is incorrect, with correct match falling below the redMaPPer selection threshold.

MCXC J2258.1+2055: Matchings differ. Membership match is clearly correct.

MCXC J0943.5+1640: Matchings differ. Membership match is clearly correct.

MCXC J1235.1+4117: No cylindrical match. Membership match is clearly correct.

MCXC J1337.8+3854: No membership matching. X-ray clusters has no nearby bright galaxies, which is very unusual. We assume this cluster is unmatched, and note this may be an X-ray false detection.

MCXC J1254.8+255: No membership match. Correct match falls below redMaPPer selection threshold, so cluster should be unmatched.

MCXC J0943.7+1644: Matchings differ. Membership match is clearly correct.

MCXC J1436.9+5507: No cylindrical match. Membership match is a larger foreground cluster. Cluster does not pass redMaPPer selection threshold, so it should be unmatched.

MCXC J1254.6+2545: No cylindrical match. Membership match is clearly correct.

There are no clusters where the matchings differed in the ACCEPT, Mantz, and Planck reference cluster catalogs.

B. NOTES ON UNMATCHED CLUSTERS

Below is the complete list of unmatched clusters in our reference catalogs.

XCS:

XCS J0943.9+1641: The cluster was assigned a high richness because it neighbors a richer system that is not included in XCS. The cluster should be unmatched.

MCXC:

MCXC J0751.4+1730: This cluster was identified as a catastrophic photometric failure, and was therefore unmatched by hand in our visual inspection.

MCXC J0159.3+0030: This is a very rich cluster, but gets masked out from redMaPPer because at its optical center, more than 20% of the cluster is lost to the galaxy mask. In other words, the cluster doesn't formally fall within the angular redMaPPer selection region.

MCXC J0159.3+0030: Like the previous cluster, this system is lost to the galaxy mask since at its optical center, more than 20% of the cluster is lost to the galaxy mask. Thus, the cluster is formally not within the angular redMaPPer selection region.

There are also 4 clusters that are matched to redMaPPer systems, but fall below our selection threshold at the redMaPPer center/redshift. These are MCXC J0927.1+5327, MCXC J1340.9+3958, J1011.0+5339, and J1334.5+3756.

Planck ESZ:

PLCKG96.9+52.5: Like the previous cluster, this system is lost to the galaxy mask since at its optical center, more than 20% of the cluster is lost to the galaxy mask. Thus, the cluster is formally not within the angular redMaPPer selection region.

There are no unmatched clusters in the ACCEPT and Mantz reference catalogs.

C. NOTES ON REDSHIFT OUTLIERS

Below is the complete list of redshift outliers between all reference cluster catalogs.

XCS Outliers:

XMMXCS J0921.2+3701: Cluster is miscentered in optical based on X-ray data. The redMaPPer cluster center has a spectroscopic redshift $z_{\text{spec}} = 0.235$, in agreement with the redMaPPer photometric redshift. It seems likely that the reference redshift is incorrect, but a spectroscopic redshift of the correct central galaxy is unavailable.

MCXC Outliers:

MCXC J1621.0+2546: SDSS spectra confirm redMaPPer redshift.

MCXC J1421.6+3717: SDSS spectra confirm redMaPPer redshift.

MCXC J1621.0+2546: SDSS spectra confirm redMaPPer redshift.

MCXC J1017.5+5934: SDSS spectra confirms redMaPPer redshift.

MCXC J0935.4+0729: SDSS spectra confirm redMaPPer redshift.

MCXC J2135.2+0125: SDSS spectra unavailable, but visual inspection strongly suggests reference redshift is incorrect.

MCXC J0809.6+2811: redMaPPer redshift compromised by bad SDSS photometry from a nearby star.

MCXC J0826.1+2625: Our photometric redshifts at the redMaPPer center and the reference cluster center disagree. The cluster is properly centered by redMaPPer, and the corresponding photometric redshift is correct based on that galaxy's spectroscopic redshift.

MCXC J0847.1+3449: Optical inspection reveals the redMaPPer match is in fact a foreground cluster in the vicinity of the X-ray cluster. The correct cluster match is detected by redMaPPer, but falls below the richness threshold, likely due to masking by the foreground cluster. This cluster should be formally unmatched. We update our matchings appropriately, and remove this system from the list of matched clusters.

MCXC J1011.4+5450: The X-ray center falls between two galaxy clumps. Both clumps are the same photometric redshift $z_{\lambda} \approx 0.35$, suggesting that the reference redshift $z_{\text{ref}} = 0.294$ is incorrect.

MCXC J0943.1+4659: SDSS spectra confirm MCXC redshift.

MCXC J0124.5+0400: SDSS spectra confirm MCXC redshift.

MCXC J1447.4+0827: This cluster has a spectacular star bursting galaxy at its center, with $z_{\text{spec}} = 0.375$, confirming the redMaPPer redshift.

ACCEPT Outliers:

MACS J2211.7-0349: No SDSS spectra, but redshift value in Mantz et al. (2010b) confirms the redMaPPer redshift.

Abell 1763: SDSS spectra confirm redMaPPer redshift.

Mantz Outliers:

400d J0809.6+2811: This cluster is the same as MCXC J0809.6+2811 (above). The redMaPPer redshift is compromised by bad SDSS photometry from a nearby star.

Planck ESZ Outliers:

PLCKG56.0-34.9: This cluster is the same as MCXC J2135.2+0125. Spectra are unavailable, but visual inspection strongly suggests the MCXC redshift is incorrect.

D. NOTES FROM CENTERING ANALYSIS

XCS:

XCS J2239.4-0547: This is one of a pair of galaxy clusters at the same redshift, the second being XCS J2239.7-0543. Each XCS system has $T_X = 2.8$, but the pair is identified as a single redMaPPer cluster. Since even the X-ray center is ambiguous, we remove these cluster from the centering analysis.

XMMXCS J1052.4+4419: There are two clusters near this location at spectroscopic redshift $z = 0.44$ and $z = 0.50$. The latter is the XCS system. redMaPPer finds both clusters, but the XCS system is heavily masked by the lower redshift objects, and falls below the detection threshold, so it is difficult to determine whether this system is a centering failure or not. We remove the system from our centering study.

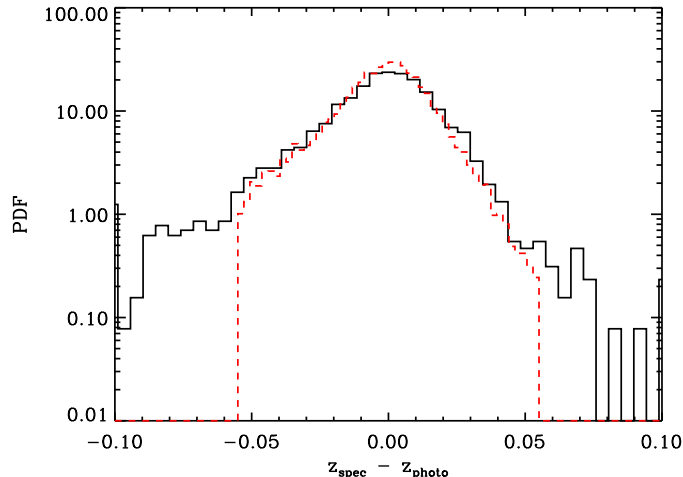


Figure 12. Distribution of the redshift offset $z_{\text{spec}} - z_{\text{photo}}$ for the Wen et al. (2012) catalog, measured using redshifts exclusive to DR9 (solid black histogram) and redshifts from the DR8 release (red histogram). All clusters in the redshift range $z_{\text{photo}} \in [0.1, 0.5]$ are included. The distribution of the DR8 redshift offsets is clearly artificially truncated at $|\Delta z| \leq 0.055$, thereby removing the tails of the distribution.

ACCEPT:

Abell 115 (3C 28.0): The cluster has a N and S component. redMaPPer is centered on the S component, but ACCEPT centers the cluster on the N component, which dominates the X-ray emission. However, both weak lensing Okabe et al. (2010); AMI Consortium (2011) and dynamical data Barrena et al. (2007) reveal 2 additional substructures both support the S component being the dominant one, by a factor of $\approx 4 - 10$ in mass, which led AMI Consortium (2011) to suggest that the X-ray emission from the N component is in fact dominated by emission associated with the ratio source 3C 28. The S component is also clearly dominant in the optical. Consequently, we assume this clusters was correctly centered, but caution that our conclusion may be incorrect due to correlated scatter between optical richness, weak lensing mass, and velocity dispersion.

Abell 1758: A1758 has been extensively studied (David & Kempner 2004; Okabe & Umetsu 2008; Haines et al. 2009; Durret et al. 2011a). It is typically split into two components — A1758N and A1758S — separated by ≈ 2 Mpc. Both components are identified as independent clusters by redMaPPer, but it is only A1758N which is included in ACCEPT. A1758N is itself a merging system, with X-ray and optical data suggesting that the N component dominates, implying redMaPPer correctly identified the central galaxy of this cluster. Our central galaxy coincides with the X-ray peak, but is significantly offset from the X-ray centroid.

Abell 1914: This is a complicated merging system with a highly irregular mass distribution (Okabe & Umetsu 2008; AMI Consortium 2011). Both X-ray and SZ data suggest the brightest cluster galaxy is the center of the dominant component, though the weak lensing κ peak of the NE component appears to be slightly higher (but less extended). We follow Okabe & Umetsu (2008) and tentatively associate the SW component as the dominant clump, which makes Abell 1914 a redMaPPer centering success.

Abell 370: There are two comparably bright cD galaxies near the X-ray center of almost equal brightness ($\Delta m = 0.05$). Contrary to the other times when we were faced with a similar decision, in this case we assigned the dimmer galaxy as the correct center, based on the curvature of an obvious giant arc. Our visual choice agrees with the redMaPPer center.

Mantz:

MACS J2311.5+0338: Cluster has distinct NE and SW components. redMaPPer centered on the NE, but X-rays indicate that the SW component is dominant.

E. EVIDENCE FOR SPECTROSCOPIC CUTS IN THE WHL CATALOG

As noted in section 8.1, we evaluate the redshift performance of the WHL catalog using clusters with spectroscopic redshifts exclusive to DR9. Our motivation for excluding all DR8 photo-zs from consideration is shown in Figure 12, where we compare the distribution of the redshift offset $z_{\text{spec}} - z_{\text{photo}}$ as evaluated using DR8 spectra (red dashed histogram), to that obtained using redshifts exclusive to DR9 (solid black histogram). We note that the redshifts exclusive to DR9 were not publicly available at the time the Wen et al. (2012) catalog was published. It is clear from the figure that the distribution for the DR8 sub-sample is artificially truncated at $|z_{\text{spec}} - z_{\text{photo}}| \leq 0.055$. Given that there is clear evidence this sub-sample of galaxy clusters was subject to a spectroscopic redshift cut, we evaluate the redshift performance of the WHL algorithm using only clusters with spectroscopy exclusive to DR9.